© 2020. Published by The Company of Biologists Ltd | Journal of Cell Science (2020) 133, jcs240754. doi:10.1242/jcs.240754

TOOLS AND RESOURCES

A toolbox of stable integration vectors in the fission yeast *Schizosaccharomyces pombe*

Aleksandar Vještica*,‡, Magdalena Marek*, Pedro Junior Nkosi, Laura Merlini, Gaowen Liu, Melvin Bérard, Ingrid Billault-Chaumartin and Sophie G. Martin‡

ABSTRACT

Schizosaccharomyces pombe is a widely used model organism to study many aspects of eukaryotic cell physiology. Its popularity as an experimental system partially stems from the ease of genetic manipulations, where the innate homology-targeted repair is exploited to precisely edit the genome. While vectors to incorporate exogenous sequences into the chromosomes are available, most are poorly characterized. Here, we show that commonly used fission yeast vectors, which upon integration produce repetitive genomic regions, give rise to unstable genomic loci. We overcome this problem by designing a new series of stable integration vectors (SIVs) that target four different prototrophy genes. SIVs produce non-repetitive, stable genomic loci and integrate predominantly as single copy. Additionally, we develop a set of complementary auxotrophic alleles that preclude false-positive integration events. We expand the vector series to include antibiotic resistance markers, promoters, fluorescent tags and terminators, and build a highly modular toolbox to introduce heterologous sequences. Finally, as proof of concept, we generate a large set of ready-to-use, fluorescent probes to mark organelles and cellular processes with a wide range of applications in fission yeast research.

This article has an associated First Person interview with the first author of the paper.

KEY WORDS: Fission yeast, *Schizosaccharomyces pombe*, Genome stability, Integrative vector, Molecular genetics

INTRODUCTION

The fission yeast *Schizosaccharomyces pombe* is a well-established model organism for studying diverse aspects of cellular biology. It continues to play a critical role, for instance in the discovery of fundamental aspects of cell cycle control, chromosome biology, signalling and cytoskeleton dynamics (Hoffman et al., 2015). Decades of research have yielded versatile molecular methods to control the expression of native and foreign genes in this species.

The ability to transform cells with genetic material and create transgenic lines is critical in biological research. Foreign DNA fragments are easily delivered to *S. pombe* cells, where they have one of two fates. First, circular DNA plasmids can be maintained as episomal fragments, provided they contain an autonomous replicating sequence (ARS) (e.g. the pREP series; Craven et al., 1998; Forsburg and Sherman, 1997; Maundrell, 1993; Moreno et al., 2000). However, these episomal plasmids do not contain centromeric segments, because *S. pombe* centromeres are complex 100 kb-long sequences, distinct from the point centromeres of the budding yeast *S. cerevisiae* (Clarke, 1990; Yamagishi et al., 2014). For this reason, such circular plasmids segregate randomly during division, leading to variable copy numbers in the population and the need for continuous selective pressure to prevent plasmid loss. Second, because homologous recombination is highly efficient, linear DNA fragments can easily integrate at desired genomic loci. This allows precise genome editing and direct gene manipulation at their native locus, the method of choice to alter gene function in near-physiological conditions. It also allows for integration of linearized 'integrative' plasmids, for instance containing foreign DNA, to placeholder genomic loci. The most common integrative vectors typically carry a single homology region. Plasmid linearization within this region enables homology-directed repair to target the vector to the desired genomic location (Keeney and Boeke, 1994; Matsuyama et al., 2004; Maundrell, 1993). However, this system suffers from the problem that integration leads to duplication of sequences on either side of the integrated vector (Siam et al., 2004), which can further recombine and lead to either amplification or deletion of the integrated fragment. This is especially noticeable if the insert alters cell fitness, and can cause reproducibility issues between experiments. A few integrative plasmids that should not lead to the formation of genomic copies have been developed, but their stability has not been directly probed (Fennessy et al., 2014; Kakui et al., 2015).

Here, we present a series of easy-to-use, modular integrative vectors that insert into the genome as a stable, single copy, without formation of genomic repeats. The basic elements included in our vector series are: a bacterial replication origin and ampicillin resistance (AmpR) sequence, allowing for plasmid amplification in bacteria, one or two multiple cloning sites (MCS), a sequence targeting the construct to one of four different chromosomal locations (*ade6*, *ura4*, *lys3* or *his5*), which confers prototrophy post transformation, and an optional drug resistance marker. We further expand this basic vector backbone by including various promoter, fluorescence tag and terminator sequences, allowing for expression of any gene of interest at desired levels.

The most popular inducible promoter in fission yeast is based on the strong *nmt1* ('no message in thiamine') promoter and its two attenuated versions that carry mutations in the TATA box – namely *nmt41* and *nmt81* (Basi et al., 1993; Maundrell, 1990; Maundrell, 1993). The *nmt* promoters display a strong induction fold after de-repression (estimated at ∼80-fold for *nmt1*; Basi et al., 1993), but their maximal induction time exceeds 15 h and is not completely synchronous in the population (Maundrell, 1990; Watson et al., 2013). The *urg1* promoter is also inducible and shows a strong

Department of Fundamental Microbiology, University of Lausanne, Biophore building, CH-1015 Lausanne, Switzerland.
*These authors contributed equally to this work

‡Authors for correspondence (aleksandar.vjestica@unil.ch; sophie.martin@unil.ch)

A.V., 0000-0002-3095-4169; M.M., 0000-0001-6901-920X; L.M., 0000-0002-8355-9541; G.L., 0000-0002-6520-5547; S.G.M., 0000-0002-5317-2557

Received 18 October 2019; Accepted 24 November 2019

Journal of Cell Science (2020) 133, jcs240754. doi:10.1242/jcs.240754

induction in the presence of uracil (but also upon nitrogen starvation), with faster kinetics: maximal transcript levels occur 30 min post induction and decrease rapidly after uracil removal with both states being stable for at least 24 h (Watt et al., 2008). However, at non-native integration sites, the off-state of p^{urg1} is strongly elevated, reducing the dynamic range of induction (Watson et al., 2013). The most widely used constitutive promoter is the strong p^{adh1}, and a few others of similar or slightly weaker strength have been described (Matsuyama et al., 2008; Siam et al., 2004). Here, we make use of the known inducible promoters (*nmt1*, *nmt41*, *nmt81*, *urg1*) and a series of constitutive promoters (*cdc12*, *pom1*, *rga3*, *pak1*, *act1* and *tdh1*) that lead to GFP expression over three orders of magnitude.

Our stable integration vector (SIV) series was built in a highly modular way. For instance, fluorescence tagging vectors allow for both N- and C-terminal tagging of the construct of interest. As multicloning sites are identical in all the vectors, quick exchange of elements allows for further expansion of the toolbox. We demonstrate the stable and single-copy integration of the SIV series and fully describe promoter strength. We introduce three new auxotrophic deletion alleles of the target genomic integration sites (at *ade6*, *lys3* and *his5*), which abrogate false-positive transformants. Finally, using the SIV series, we generate a panel of fluorescent bio-markers in three compatible wavelengths (mTagBFP2, sfGFP or GFP and mCherry), labelling commonly studied cellular organelles, structures and processes. We expect these tools to be a valuable asset to all researchers using the fission yeast system.

RESULTS

The presence of two regions of homology to target sequences promotes stability of integrants and avoids tandem integration events

In fission yeast, homologous recombination is efficient and has been used for decades to introduce exogenous constructs at defined genomic loci through integration of linearized plasmids. Traditional integrative vectors contain the wild-type sequence of a prototrophic selection marker, such as *leu1+* or *ura4+* in the case of the widely used pJK148 and pJK210 vectors, respectively. Upon linearization, plasmids can restore prototrophy upon recombination into corresponding genomic loci, which in the parental genome carry inactivating point mutations leading to auxotrophy, such as *leu1-32* or *ura4-294* (Keeney and Boeke, 1994). While efficient and site-specific, these recombination events also lead to up to 20% of transformants with multiple integration events [two or more copies integrated in tandem in the genome (Keeney and Boeke, 1994)]. Even upon integration of the plasmid in single copy, the procedure leads to duplication of the auxotrophic marker genomic sequence (Fig. 1A), which can cause locus instability. Indeed, we observed that strains in which fluorescent biosensors were introduced on such integrative vectors occasionally gave rise to cells lacking the probe. While mutations in the gene encoding the probe could lead to apparent loss of signal, spontaneous mutations in wild-type fission yeast are rare (2×10^{-10} for base substitutions; Farlow et al., 2015) and thus unlikely to account for the recurrent events we observed with different probes and strains. Instead, we speculated that the probe was lost because of recombination between the genomic repeats created by integrative vectors (Fig. 1A).

To quantify the instability of pJK210 integrants, we introduced a nourseothricin resistance cassette (natMX) into the pJK210 vector, which carries a *ura4+* gene as a selection marker. We transformed auxotrophic cells carrying the point mutation *ura4-294* and selected for uracil prototrophs with nourseothricin resistance. We subsequently cultured these transformants in non-selective medium for 3 days and plated 1.4×10^{7} cells onto medium containing 5-fluoroorotic acid (5-FOA), which acts as a counter selection against the *ura4+* gene (Fig. 1C). Inactivation of *ura4* in pJK210 integration strains occurred at a frequency that was three orders of magnitude above the rates we observed for a wild-type prototroph strain (Fig. 1D, proportion was $4.1\times10^{-4}\pm1.6\times10^{-4}$ for pJK210 transformants and $1.4\times10^{-7}\pm2.5\times10^{-7}$ for wild-type cells, n=6, mean±s.d.). Furthermore, 58.0±20.3% of transformants with an inactivated *ura4* gene also lost the resistance to nourseothricin, suggesting loss of vector sequences. Our results suggest that recombination between the repeats introduced upon pJK210 integration are a likely cause for the instability of the integrated construct.

We aimed to create an SIV by developing a new pUra4^{AfeI} vector (Fig. 1B), which integrates at the *ura4* locus without creating genomic repeats. pUra4^{AfeI} linearization at the *AfeI* site produces two separate homology regions (Fig. 1B). The first homology arm contains the functional *ura4* cassette [5′ region, open reading frame (ORF), 3′ region]. The second arm is homologous to sequences just downstream of the *ura4* cassette (3″ region). Integration of the linearized fragment relies on recombination at both homology regions, which replaces the genomic *ura4* sequences and thus avoids repeat formation (Fig. 1B). Integration is confirmed using three diagnostic PCRs, which probe for correct integration on both sides of the linearized vector and for an increase in the distance between the 3′ and 3″ *ura4* genomic regions (Fig. S1; see Materials and Methods for details). We introduced the natMX6 cassette using the pUra4^{AfeI} vector into the *ura4-294* mutant strain. Nourseothricin-resistant, uracil prototroph transformants exhibited a stable *ura4* locus with a frequency of cells resistant to 5-FOA similar to that of wild-type prototrophs (Fig. 1D). Importantly, all of the 5-FOA-resistant clones that arose in the population maintained the nourseothricin resistance, indicating continued presence of vector sequence (Fig. 1C). We conclude that exogenous DNA can be stably introduced in the genome at a defined locus by avoiding the formation of genomic repeats.

To monitor the presence or absence of genomic repeats upon vector integration, we used quantitative PCR (qPCR). We first characterized the sensitivity of the assay by examining strains carrying the *ura4* gene in single (wild-type *ura4+*), two (*pak2Δ:ura4+ ura4+*) and three (*myo51Δ:ura4+ pak2Δ:ura4+ ura4+*) copies. The qPCR results clearly reflected an increase in *ura4* copy number as compared to the *act1* gene, which we used as a reference locus (Fig. 1E). We then assayed the genomic DNA of 12 clones obtained by transforming pJK210 and pUra4^{AfeI} vectors. The majority of pJK210 transformants showed two copies of the *ura4* gene, consistent with duplication of the *ura4* locus upon vector integration. In addition, one clone showed a more than 3-fold *ura4* signal, revealing a multiple integration event (Fig. 1E), consistent with previous data showing that pJK210 can integrate in multiple tandem copies (Keeney and Boeke, 1994). In the case of pUra4^{AfeI}, all but one clone showed *ura4* present in single copy, with one clone possibly present in two copies (Fig. 1E). Thus, pUra4^{AfeI} integrates in the genome without causing duplication. In addition, these results show that the majority of transformants result in single-copy integrations, consistent with the vector design.

To quantify the rates of false-positive clones produced with the pUra4^{AfeI} vector (e.g. clones that are uracil prototrophs but have not integrated the vector), we used pUra4^{AfeI} to introduce a locus encoding high levels of superfolder (sf)GFP into *ura4-294* cells. Blue light illumination showed that transformant colonies obtained after uracil selection were green due to sfGFP expression. However, sfGFP expression was absent from 5.2±2.1% (mean±s.d.) of transformants (Fig. 1F, top panel; Fig. 1G). False-positive

Journal of Cell Science (2020) 133, jcs240754. doi:10.1242/jcs.240754

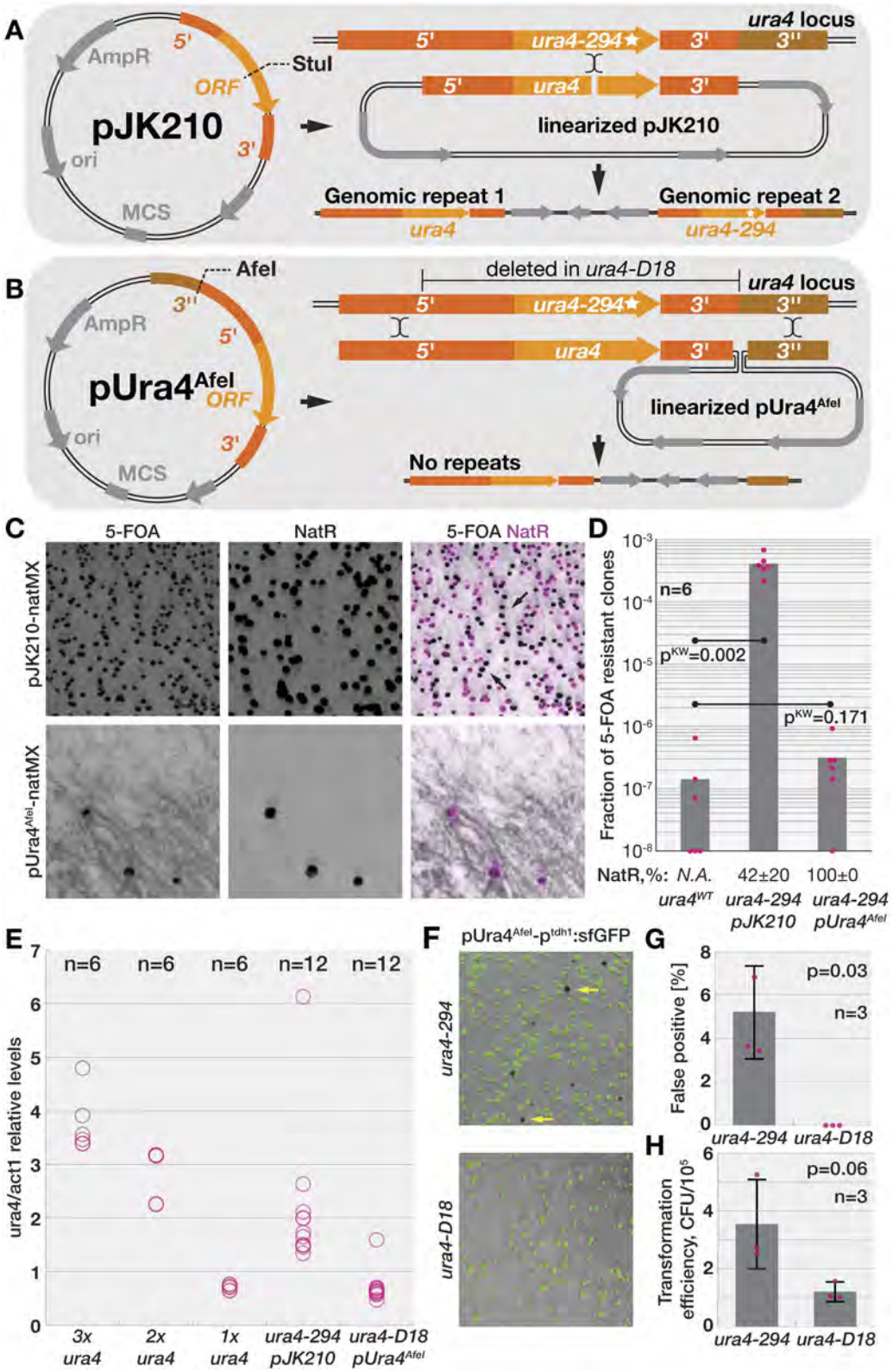

Fig. 1. See next page for legend.

transformants may arise from a double crossover that only spans the *ura4-294* point mutation and restores the wild-type *ura4+* gene without integrating any vector-specific sequences. The commonly used *ura4-D18* mutant allele (Grimm et al., 1988) has the entire open reading frame of the *ura4* gene deleted, leaving homology only to the tips of homology arms in the linearized pUra4^{AfeI} (Fig. 1B). Transformation of pUra4^{AfeI} into cells harboring *ura4-D18* resulted in false-positive rates below the detection limit of our assay (~0.2%; Fig. 1F, bottom panel; Fig. 1G). While the routine transformation protocol still yielded hundreds of transformants, the

Journal of Cell Science (2020) 133, jcs240754. doi:10.1242/jcs.240754

Fig. 1. Two homology arms promote stable vector integration into the chromosome. (A) Schematic of the pJK210 vector (left panel) and its integration into the genomic *ura4-294* locus post-linearization (right panel). 5′, ORF and 3′ refer to *ura4* gene sequences as indicated in the genomic locus. AmpR encodes for ampicillin resistance and ori stands for the ColE1 bacterial replication origin. The unlabelled arrow represents an F1 replication origin. A single site crossover leads to the integration of the vector and duplication of the target locus (for detailed explanation see Jasin and Rothstein, 2013; Lee et al., 2014). (B) Schematic of the pUra4^{AfeI} vector (left panel) and its integration into the genomic *ura4-294* locus post-linearization (right panel). 3″ refers to the indicated sequences downstream of the 3′ segment. Note that the two homology regions are separated by the *Afe*I linearization site. Crossovers at both homology arms integrate the vector into the genome without duplication of the target locus. Note that the *ura4-294* point mutation in the ORF can be rescued by a single crossover that does not lead to vector integration. The *ura4-D18* mutant, which lacks the indicated fragment, only has homology with the distal ends of the homology arms, ensuring that the vector integrates along with the *ura4+* selection cassette. (C) Assessment of integrant stability. Yeast strains transformed with the plasmids pJK210 (top) or pUra4^{AfeI} (bottom) in which the *ura4+* and *natMX6* selection cassettes were introduced were grown in non-selective conditions for 3 days and 1.4×10^7 cells were plated on medium with 5-FOA (left panels), which is lethal to cells encoding a functional *ura4+* gene. After colonies developed, we replica plated them onto medium containing nourseothricin (middle panels). False-coloured images from the two plates are overlaid on the right panel. Note that numerous colonies develop if selection markers were originally introduced using pJK210 but not pUra4^{AfeI} vector. Approximately half of the 5-FOA-resistant clones from the pJK210 integration also lost the natMX6 cassette, which was maintained in all clones obtained from pUra4^{AfeI}-transformed strain. (D) The graph quantifies the proportion (fraction) of 5-FOA-resistant clones upon plating 1.4×10^7 cells. The percentage of cells with nourseothricin resistance is shown at the bottom of the graph. Statistical significance (p^{KW}) between indicated samples is reported as *P*-values from the Kruskal–Wallis test. (E) qPCR results comparing the relative abundance of *act1* and *ura4* genomic loci for strains containing the indicated number of *ura4* loci, and for 12 strains obtained by transformation with indicated plasmids each. (F) Measure of false-positive integrations. The indicated *ura4* mutant alleles were transformed with a cassette for sfGFP expression cloned into the pUra4^{AfeI} vector and selected for growth on medium lacking uracil. The colonies that developed were imaged in white light (greyscale image) and green fluorescent channel (green) and the images were overlaid. The arrows point to false-positive colonies that lack the fluorescent marker but contain the functional *ura4* cassette. (G) Quantification of percentages of false-positive colonies observed in F. (H) Quantification of overall transformation efficiencies observed in F. The *P*-values in G and H were calculated using the paired Student's *t*-test. In all graphs, points report individual data points, bars report average values from multiple replicates and error bars report standard deviation.

transformation efficiency of pUra4^{AfeI} into the *ura4-D18* strains decreased 3-fold as compared to *ura4-294* [Fig. 1H; $1.2\pm0.3\times10^{-5}$ and $3.5\pm1.5\times10^{-5}$ colony-forming units (CFU)/10^5 cells for the *ura4* deletion and point mutant, respectively]. We conclude that restricting homology with the genome to the edges of the linearized vector leads to decreased rates of false-positive transformants.

Taken together, we show that the pUra4^{AfeI} vector can be used to reliably integrate sequences in single copy into the genome without producing genomic repeats. We find that minimal numbers of false-positive transformants are achieved when targeting the *ura4-D18* deletion mutant locus.

A series of SIVs

Experiments increasingly rely on simultaneously monitoring multiple probes and markers. We thus developed a series of vectors similar to pUra4^{AfeI} but targeting the additional *ade6*, *lys3* and *his5* loci. For each locus, we cloned the plasmid backbone with one homology arm that contains the 5′ region, ORF and 3′ region, which is preceded by a linearization site and a second homology arm targeting the downstream 3″ region (Fig. 2A). We named these plasmids pAde6^{PmeI}, pLys3^{BstZ17I} and pHis5^{StuI}.

We first tested the stability of pAde6^{PmeI}, pLys3^{BstZ17I} and pHis5^{StuI} integrants. To this aim, we simultaneously introduced both *ura4+* and antibiotic resistance cassettes into the vectors, linearized them and transformed them into *ura4-D18* uracil auxotroph yeast cells. Note that these strains were prototroph for adenine, lysine and histidine. We selected clones that were both uracil prototroph and antibiotic resistant. We then monitored the stability of the integrated locus by counter-selecting against *ura4+* using 5-FOA. The inactivation of the *ura4* gene occurred at frequencies similar to that found in wild-type cells (Fig. 2B, proportion of $7.1\times10^{-8}\pm12.4\times10^{-8}$ for the *ade6* locus, $3.3\times10^{-8}\pm5.8\times10^{-8}$ for the *his5* locus, and below the detection limit for the *lys3* locus), suggesting it was due to spontaneous mutations. Importantly, the strains with an inactivated *ura4* gene invariably maintained the antibiotic resistance (Fig. 2B). We concluded that, as with pUra4^{AfeI}, transformation with pAde6^{PmeI}, pLys3^{BstZ17I} and pHis5^{StuI} produces stable integrants. We note that we also attempted the same strategy to target the *leu1* locus with pLeu1^{StuI} but found that the selective marker was rapidly lost in most transformants after removing the selective pressure. While we did not pursue this issue further, a possible explanation is that the *leu1* genomic region contains a replication origin, which allows the plasmid to exist as an unstable, episomal element.

We proceeded to assess the rate of false-positive transformants with the newly designed vectors. To this aim, we introduced a cassette that expresses high levels of sfGFP in pAde6^{PmeI}, pLys3^{BstZ17I} and pHis5^{StuI} and integrated the vectors into the genome of *ade6-M210*, *lys3-37* or *his5Δ1* auxotrophic strains, respectively. After selection for prototrophs, we could distinguish colonies that do and do not express the fluorophore, and thus determine the proportion of false positives (Fig. 2C,D; 8.2±2.6% false positives for *ade6-M210*, 5.6±1.7% for *lys3-37* and 3.8±2.0% for *his5Δ1* alleles, mean±s.d.). We suspected that we could decrease the false-positive rates by designing new auxotrophic deletion alleles (detailed in Materials and Methods). Specifically, we engineered *ade6-D19*, *lys3-D20* and *his5-D21* mutants that lack most of the ORF and the immediate 3′ region, and thus must recombine at both upstream and downstream regions to introduce the selection marker into the genome. Using these strains to integrate the fluorescent cassette into the genome almost completely abolished the appearance of false-positive clones (Fig. 2C,D; 0.21±0.19% of false positives for *ade6-D19*, below detection limit for *lys3-D20* and $6.5\times10^{-3}\pm11.3\times10^{-3}$% for *his5-D21* alleles). Using our new deletion alleles had little effect on overall transformation efficiencies (Fig. 2E). Finally, we used our plasmids to integrate the *ura4+* cassette at either the *ade6*, *lys3* or *his5* locus of the *ura4-D18* mutant. This allowed us to then monitor the number of plasmid integrants by the qPCR assay described above, which compared relative levels of *ura4* and *act1* sequences in the genome (Fig. 2F). We tested 12 transformants with each plasmid and found that all underwent a single integration event.

Taken together, our results indicate that the pAde6^{PmeI}, pLys3^{BstZ17I} and pHis5^{StuI}, as well as pUra4^{AfeI}, can be used to introduce desired sequences into the fission yeast genome almost without any copy number variation. Furthermore, using auxotrophic deletion alleles with restricted regions of homology ensures almost negligible rates of false-positive transformants.

Expanding the usage of the SIVs

Using the above-described vectors requires target strains to be auxotroph for the required loci. To circumvent this requirement, we decided to introduce additional dominant selection markers. We cloned the antibiotic resistance cassettes kanMX6, natMX6, hphMX6, bleMX6 and bsdMX6 into our vectors (Bähler et al.,

Journal of Cell Science (2020) 133, jcs240754. doi:10.1242/jcs.240754

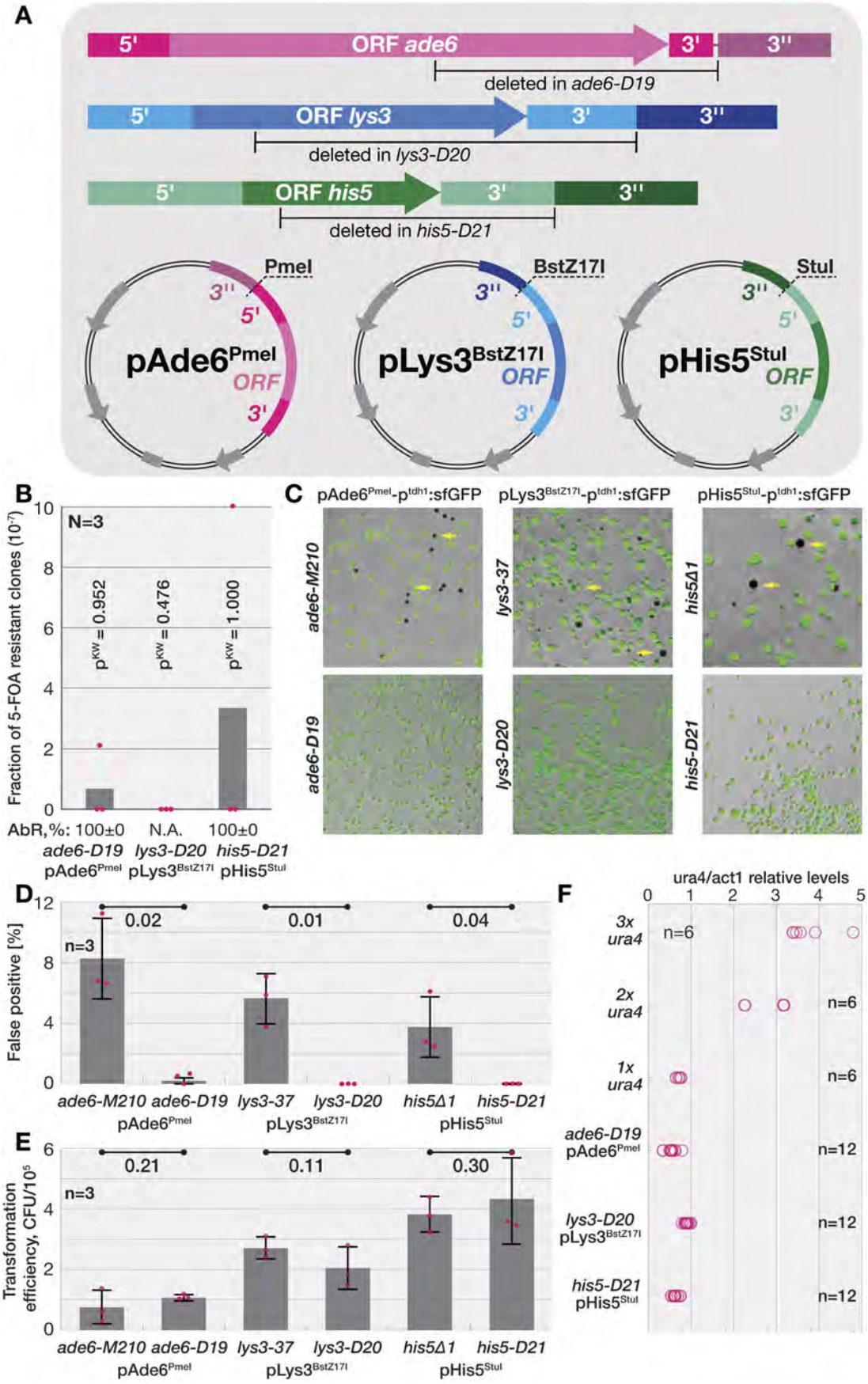

Fig. 2. See next page for legend.

Journal of Cell Science (2020) 133, jcs240754. doi:10.1242/jcs.240754

Fig. 2. Vector series for stable chromosomal integration. (A) Schematics of the genomic loci (top) targeted by the pAde6^{PmeI}, pLys3^{Bstz17I} and pHis5^{StuI} vectors (bottom). The segments that are deleted in the mutants *ade6-D19*, *lys3-D21* and *his5-D21* are also indicated. Notations are as in Fig. 1B. (B) Assessment of integrant stability. Yeast strains where the *ura4* and antibiotic selection cassettes were introduced on indicated plasmids, were grown in non-selective conditions for 3 days and plated onto medium with 5-FOA. After colonies developed, we replica plated them onto medium containing the antibiotic. The graph quantifies the proportion (fraction) of 5-FOA-resistant clones that formed upon plating 1.4×10^7 cells. The percentage of antibiotic-resistant colonies is indicated at the bottom. Statistical significance (p^{KW}) between indicated samples and the wild type is reported as *P*-values from the Kruskal–Wallis test. (C) Measure of false-positive integrations. Indicated mutant alleles were transformed with a cassette for sfGFP expression cloned into indicated vectors and prototrophs were selected. The colonies that developed were imaged in white light (greyscale image) and green fluorescent channel (green) and the images were overlaid. The arrows point to false-positive prototrophic colonies that lack the fluorescent marker. (D) Quantification of percentage of false-positive colonies observed in C. (E) Quantification of overall transformation efficiencies observed in C. *P*-values denoted on the top in D and E were calculated for indicated comparisons using the paired Student's *t*-test. (F) Quantitative PCR results comparing relative abundance of *act1* and *ura4* genomic loci for strains containing indicated number of *ura4* loci (same data as in Fig. 1E) and for 12 strains obtained by transformation with indicated plasmids that carry the *ura4* gene. Note that all transformants exhibit *ura4*/*act1* relative levels indicative of a single integration event. In all graphs, points report individual data points, bars report mean values from multiple replicates and error bars report standard deviation.

1998; Hentges et al., 2005; Kimura et al., 1994; Sato et al., 2005; Wach et al., 1994; Table S1 and Fig. 3A; details in Materials and Methods) in between two MCS to allow for their easy exchange between vectors. Transformation of linearized vectors into wild-type strains followed by antibiotic selection readily produced the desired clones. This set of vectors targeting four distinct genomic sites with five different dominant selection markers, currently composed of five distinct vectors (Table S1), can be used to clone any sequence of interest in either MCS and stably introduce it in the yeast genome in essentially any yeast strain.

In most experimental settings, control over gene expression levels is desirable. To this aim, we constructed a second set of vectors, in which ten different promoters drive the expression of sfGFP followed by the transcriptional terminator of the budding yeast *CYC1* gene. These include the inducible promoters p^{nmt1}, p^{nmt41}, p^{nmt81} and p^{urg1}, and six distinct constitutive promoters active during mitotic growth. MCSs are present in between each of the fragments to allow their easy exchange, as well as to use the plasmid for both C- and N-terminal fusion proteins with sfGFP (Fig. 3B, note that the STOP codon is within the MCS_3). Next, we compared the induction strength of the ten promoters active during mitotic growth. First, we obtained whole-cell lysates from selected strains and analysed sfGFP levels by western blotting using tubulin as a loading control. Both *nmt1* and *urg1* inducible promoters showed robust fold differences between non-induced and induced conditions, with the *nmt1* promoter expressing at higher levels (Fig. 3C). Importantly, we found that the constitutive *act1* promoter, which leads to similar expression levels as the *urg1* promoter in presence of uracil, drives similar expression levels when integrated at any of the four genomic loci (Fig. 3C). Comparison of sfGFP expression from the *act1* promoter integrated at different genomic loci by flow cytometry confirmed that the integration site does not influence expression levels (Fig. 3D). This suggests that there are no strong differences in chromatin accessibility for transcription between these four genomic loci, as observed for other loci (Allshire and Ekwall, 2015), at least in otherwise wild-type cells.

To compare the activity of other promoters driving sfGFP expression, we quantified the fluorescence detected by spinning disk confocal microscopy (Fig. 3E; see Materials and Methods for details). As observed by western blotting, the inducible promoters gave a robust expression increase in induced conditions, with the *nmt1* promoter yielding the highest expression level, followed by p^{urg1}, p^{nmt41} and p^{nmt81}. Note, however that the expression from p^{urg1} increased only ∼20-fold upon uracil addition, as previously reported (Watson et al., 2013). The *tdh1* promoter was the highest-expressing constitutive promoter, yielding sfGFP expression levels just slightly lower than the fully induced *nmt1* promoter. This is thus a good promoter for very strong constitutive expression. The *act1* promoter led to about 7-fold lower expression levels, similar to induced *urg1*. The *pak1*, *rga3* and *pom1* promoters exhibited a further 23-, 27- and 42-fold decrease in levels, respectively. The *cdc12* promoter was about 10-fold weaker, yielding barely detectable GFP levels. We were unable to reliably detect cytosolic sfGFP when expressed from the repressed *nmt81* promoter. However, this is likely due to limitations of the assay in detecting a weak cytosolic signal against background organellar fluorescence because we obtained evidence that *cdc12* and *nmt81* promoters in the off-state lead to detectable biological activity (Hachet et al., 2011 and unpublished work by S.G.M. and Iker Lamas). We further used the *act1*, *pak1*, *rga3* and *pom1* promoters, all of which lead to detectable levels of cytosolic GFP, to express Ltc1, a protein localized at ER–PM contact sites (Fig. 3F; Marek et al., 2019 preprint). The localization of Ltc1, which was difficult to detect from its native promoter, showed a more prominent localization pattern when mildly overexpressed from *pak1*, *pom1* or *rga3* promoters. Stronger overexpression from the *act1* promoter resulted in ectopic localization throughout the ER. This example illustrates how the range of promoters driving expression over three orders of magnitude will allow tweaking of gene expression levels to reveal biological insight.

In summary, we provide three sets of single-integration SIVs: (1) pUra4^{AfeI}, pAde6^{PmeI}, pLys3^{BstZ17I} and pHis5^{StuI}, which lead to stable, single-copy integrations when transformed into strains auxotroph for the corresponding marker gene (Figs 1 and 2); (2) a derived set containing additional antibiotic resistance cassettes, which also allow their integration independently of the host strain genotype in prototrophic strains (Fig. 3A); and (3) a set of vectors with ten distinct promoters to drive gene expression at defined levels (Fig. 3B). This third set also needs to be transformed into auxotrophic strains. However, we note that subcloning with *Kpn*I and *Sac*I restriction enzymes allows the introduction of a DNA fragment containing promoter, sfGFP and MCSs from the third plasmid set into the second set of vectors next to the antibiotic resistance cassette (see section on 'Recommendations for use of the vectors' at the end of the Discussion for guidelines and further examples of modularity). This exemplifies the modularity of the set of plasmids we created and their possible expansion.

Using single-copy SIVs to express live-cell biology probes

Synthetic probes are routinely used in cell biology to monitor molecular dynamics and activity. For reliable quantifications and phenotype comparisons, it is imperative that probe levels be comparable between samples. Because our single-integration vectors show an invariant copy number, we used them to introduce a number of fluorescent markers into cells (Fig. 4). We used different loci and antibiotics, which allows to quickly combine multiple probes in the same cell by genetic crosses. Furthermore, we used three distinct fluorescent tags, sfGFP (Pédelacq et al., 2006), mCherry (Snaith et al., 2005) and the blue fluorophore mTagBFP2 (Subach et al., 2011), which produces a signal that is efficiently

Journal of Cell Science (2020) 133, jcs240754. doi:10.1242/jcs.240754

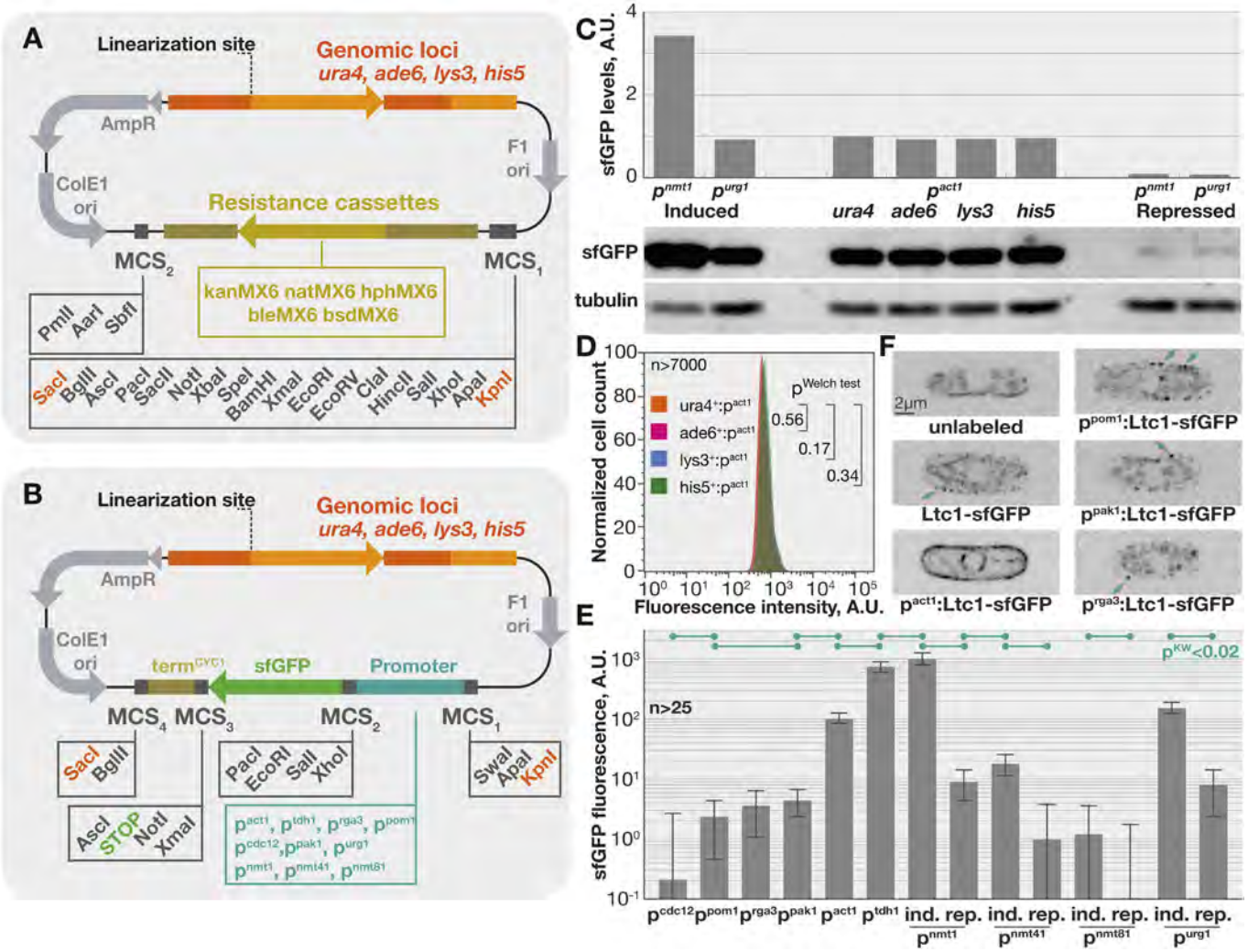

Fig. 3. Expanding the SIV toolbox. (A) Schematics of cloned vectors with indicated genomic-targeting loci (orange), antibiotic resistances (mustard) and multiple cloning sites (MCS_x). Note that not all sites are unique in all vectors. Complete vector sequences are provided in Figshare Source Data D1 to plan cloning. (B) Schematics of cloned vectors with indicated genomic targeting loci (orange), promoters (turquoise) and MCS. The STOP codon is placed between restriction enzyme sites, which allows to use the vectors for both N- and C-terminal sfGFP tagging. Note that not all sites are unique in all vectors, and that *Kpn*I and *Sac*I (highlighted) can be used to shuttle the entire constructs between vectors of this and the series presented in (A). (C) Quantification (top panel) of western blots against sfGFP (middle panel) and tubulin (bottom panel, loading control) performed on lysates obtained from cells where sfGFP was expressed from the indicated promoters. (D) Fluorescence profiles obtained by flow cytometry from cells with indicated genotypes. Note that there are no significant differences in expression of sfGFP from the *act1* promoter integrated at any of the four different genomic loci as suggested by the Welch test *P*-values that are also reported. (E) Quantification of fluorescence emitted by the sfGFP that was expressed from the indicated constitutive, induced and repressed promoters. Bars report mean values from multiple cells and error bars report standard deviation. The turquoise lines on the top of the graph indicated samples which differ with *P*-values lower than 0.02 according to the Kruskal–Wallis test. (F) Micrographs of Ltc1–sfGFP expressed from indicated promoters of different strengths and imaged with indicated exposure times. Please note that fluorescent foci (arrows) are barely notable above cell autofluorescence when Ltc1–sfGFP is expressed from the native *ltc1* locus but become clearly evident when using the *pom1*, *rga3*, or *pak1* promoters. Also note that using the strong *act1* promoter results in ectopic localization throughout the ER.

separated from GFP and mCherry by standard DAPI filters (see Materials and Methods). We used strong promoters to drive expression of the cytosolic blue, green and red fluorophore (Fig. 4A), which can be used to distinguish cells when simultaneously imaging multiple strains. We also placed the three fluorophores under mating type-specific promoters that are active only in P-gametes (p^{map3}) or M-gametes (p^{mam1*}). This allowed us to clearly differentiate gametes during mating (Fig. 4B; Movie 1). To visualize the plasma membrane, we fused the three fluorophores to an amphipathic helix from RitC (Onken et al., 2006; Fig. 4C). We targeted each fluorophore to the nucleus using a SV40 nuclear localization sequence at either one (Fig. 4D) or both ends of the protein (Fig. 4E). To monitor active export of proteins from the nucleus, we fused sfGFP with the nuclear export sequences from Alp7 and Wis1 fission yeast proteins (Fig. 4F). To monitor nuclear envelope integrity, we expressed three copies of mTagBPF2 in tandem, whose size largely prevents its nuclear influx in wild-type cells (Fig. 4G). We note that the 3mTagBPF2 also occasionally made cytosolic foci, possibly due to self-oligomerization.

To monitor microtubules, we introduced the three fluorophores at the N-terminus of α-tubulin (*atb2*) and used its 5′ and 3′ regulatory sequences to drive expression of the construct as a second copy without perturbing the native α-tubulin locus (Fig. 4H; Movie 1). We monitored the actin cytoskeleton using the LifeAct probe (Riedl et al., 2008) fused to a red or a green fluorophore (Fig. 4I; Movie 1). We also expressed LifeAct fused to mTagBFP2, but these cells

Journal of Cell Science (2020) 133, jcs240754. doi:10.1242/jcs.240754

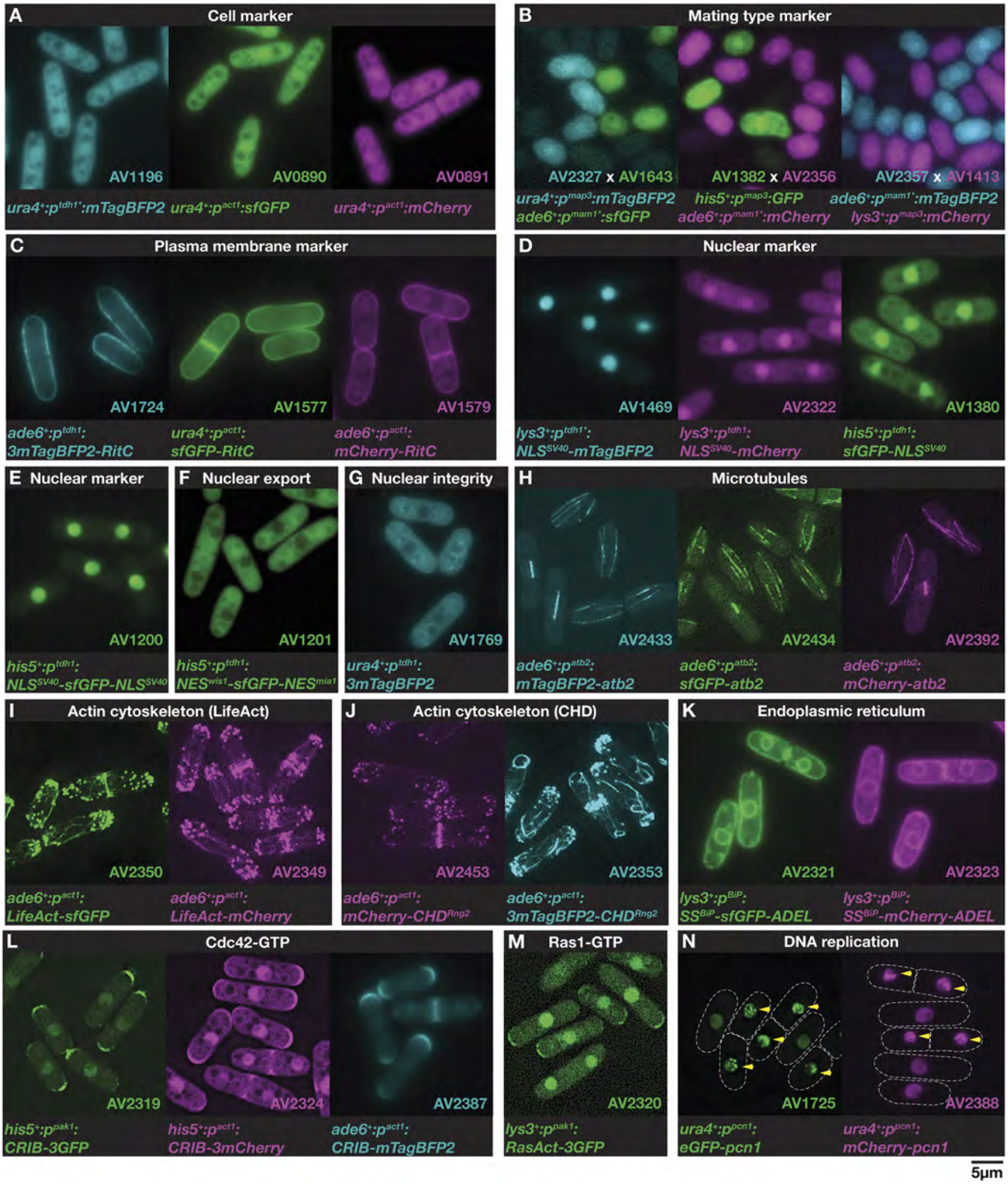

Fig. 4. Panel of cell biology probes generated using SIV toolbox. Micrographs of cells expressing green, red and blue fluorescent probes to visualize (A) cells, (B) P- and M-gametes, (C) plasma membrane, (D,E) nucleus and/or nuclear import, (F) nuclear export, (G) nuclear integrity, (H) microtubules, (I,J) actin cytoskeleton, (K) endoplasmic reticulum, (L) active Cdc42, (M) active Ras1 and (N) DNA replication foci (arrowheads). Please see the figure and the text for detail of the constructs.

exhibited growth defects (Fig. S2). As an alternative probe to visualize the actin cytoskeleton, we fused the calponin homology domain (CHD) of Rng2 protein (Wang et al., 2004) with either red or blue fluorescent protein (Fig. 4J; Movie 1). We note that cells expressing 3mTagBFP2–CHD exhibited abnormally abundant, likely stabilized actin cables. We fused the N-terminal signal

Journal of Cell Science (2020) 133, jcs240754. doi:10.1242/jcs.240754

sequence from BiP to target either sfGFP or mCherry to the ER and ensured its retention in the ER with the C-terminal ADEL sequence (Fig. 4K) (Zhang et al., 2010). We also attempted to generate a blue ER marker but did not observe any fluorescence. We expressed the CRIB–3GFP probe to monitor the GTP-bound form of the small GTPase Cdc42 using the p^{pak1} promoter as previously reported [note that this CRIB probe is 27 aa shorter than that described in Tatebe et al., (2008); Fig. 4L, left panel, Movie 1]. CRIB fused to triple mCherry or mTagBFP2 was reliably observed only when the construct was expressed using the stronger p^{act1} promoter (Fig. 4L, middle and right panels; Movie 1). We used the RasAct probe to monitor the GTP-bound form of the small GTPase Ras1 as previously reported (Merlini et al., 2018; Fig. 4M, Movie 1). Finally, to monitor cell cycle progression, green and red fluorescent proteins were fused with Pcn1, the PCNA component of the replisome, and the construct was expressed in addition to the native gene (Meister et al., 2007; Fig. 4N, Movie 1). Pcn1 produced a uniform nuclear signal except in S-phase cells undergoing DNA replication when distinct fluorescent foci representing replication factories are observed (Fig. 4N, arrowheads).

Taken together, our work provides a panel of frequently used live-cell probes that are stably expressed from a single genomic copy introduced using the vectors we developed.

DISCUSSION

We present here a large series of modular vectors for stable, single-copy integration in the fission yeast genome. This vector series expands the genetic toolbox of the popular fission yeast model *Schizosaccharomyces pombe*. For the reasons highlighted below, these vectors currently are the best tools to introduce foreign genetic material in the genome in a controlled manner. We thus encourage their wide use and further development. The vectors and strains developed herein are available from the Japanese National BioResource Project (NBRP; http://yeast.nig.ac.jp/yeast/) and the non-profit plasmid repository Addgene (https://www.addgene.org/). IDs for these repositories are provided in Table S1.

Stable and single-copy genomic integration

The controlled expression of desired genetic information is a powerful way to probe gene functionality. The popular model *Schizosaccharomyces pombe* can easily be transformed with plasmids, which have been the vector of choice for introduction of exogenous DNA. However, the fact that fission yeast centromeres are large, complex genomic elements has hindered development of centromeric plasmids such as those developed in budding yeast (Clarke and Carbon, 1980). Furthermore, fission yeast cells do not naturally carry plasmids such as the budding yeast 2 µ plasmid, which carries a partitioning system (Chan et al., 2013; Strope et al., 2015). Instead, fission yeast research has relied on either autonomously replicating episomal plasmids or on vectors integrating into the genome. Episomal vectors, such as the widely used pREP series (Maundrell, 1993), segregate randomly between daughter cells at division, which results in a copy number variation within the clonal population. Furthermore, the plasmid selection has to be continuously applied or the plasmid is rapidly lost, in particular as cells go through sexual reproduction. Most integrative plasmids (Keeney and Boeke, 1994; Maundrell, 1993) carry a single homology region that targets them into the desired locus of the genome. While efficient and precise, vector integration produces genomic repeats, which can recombine and remove the integrated segment. With a rate of plasmid sequence loss from integrant strains at $\sim 5\times10^{-4}$ over 3 days (Fig. 1D), integrated DNA that decreases cell fitness would be rapidly eliminated from the population. This is likely to be particularly prominent in genetic crosses, when genomic repeats misalign between parental chromosomes during meiotic recombination (Smith, 1976). In summary, most traditionally used vectors suffer from instability and copy-number variation.

To overcome this problem, we developed pUra4^{AfeI}, pAde6^{PmeI}, pLys3^{BstZ17I} and pHis5^{StuI} plasmids, which rely on two homology arms to integrate into the genome (Figs 1A and 2A). These vectors recombine specifically with their target genomic locus (Fig. S1B). Importantly, we have shown that integration of these vectors occurs without producing genomic repeats, and leads to a stable genomic copy that is not lost when cells are grown without selection (Figs 1C,D and 2B). The vectors also predominantly integrate as a single copy (Fig. 2F), which ensures that copy-number is not a confounding factor when comparing the biological activity of different constructs. Thus, these vectors allow reliable stable, single-copy genomic integration.

Comparison with other vector series and approaches

Integrative plasmids that rely on two homology arms have previously been developed by the Hagan/Simanis and Sato groups (Fennessy et al., 2014; Kakui et al., 2015). The first of these studies presented a highly modular series of integrative vectors that uses the Golden Gate cloning scheme to join upwards of eight fragments together in a single ligation reaction and generate vectors integrating at *lys1*, *arg1* and two intergenic regions of chromosome I and II. The second reported three vector series integrating at *leu1*, *lys1* and an hphMX cassette previously integrated at an intergenic region of chromosome III. Although the design of these plasmids with two homology arms is predicted to yield stable integrants, whether the different genomic loci chosen as integration sites exhibit similar properties to the ones we describe for *ura4*, *ade6*, *lys3* and *his5* remains to be seen, as neither stability of integration nor number of integration events have been reported. It may be unwise to assume that all sites of integration behave similarly. Indeed, we found here that targeting the *leu1* locus with a plasmid carrying two homology arms (pLeu1^{StuI}) did not systematically lead to stable genomic integration. One possible explanation is that the *leu1* sequence contains a replication origin, which may allow the cells to transiently maintain the plasmid as an episomal element if it is re-circularized by non-homologous end joining. Indeed, a potential replication origin resides at the *leu1* locus (originID: II-1983; Siow et al., 2012). The design of these previously described plasmids generates another major difference with the set of integrative plasmids described here: when vectors integrating at *lys1*, *arg1* or *leu1* are chosen, their integration leads to disruption of the target genomic site, and thus the creation of auxotrophic strains. By contrast, integration of the plasmids presented here restores (or preserves) the target locus and thus forms prototrophic transformants, which may be beneficial for the study of many physiological pathways (Alam et al., 2016). We note that it may be possible to combine the modularity of the Golden Gate cloning scheme described in Kakui et al., (2015) with the now established stability of integration and production of prototrophic transformants at *ura4*, *ade6*, *lys3* and *his5* by constructing a Golden Gate target modules donor vector using the four target integration sequences characterized here.

We designed and tested SIV plasmids properties in targeting specific genomic loci (Figs 1 and 2). These vectors are not ideally suited for modification of genes at their native locus. For this, a method of choice is the amplification by PCR of integration cassettes for gene disruption or tagging with primers that introduce

Journal of Cell Science (2020) 133, jcs240754. doi:10.1242/jcs.240754

80 bp homology arms to the genomic locus of interest (Bähler et al., 1998; Wach et al., 1994). A large panel of pFA6a-based vectors, which are widely used in the field and have been optimized for both gene deletions and gene tagging with a wide range of tags (Bähler et al., 1998; Chen et al., 2017; Gadaleta et al., 2013; Hentges et al., 2005; Sato et al., 2005; Van Driessche et al., 2005), can be used as template. For genomic loci exhibiting less efficient homologous recombination, extending the length of the homology arms is beneficial. For this, we typically construct an integrative plasmid that can be linearized between two homology regions to either side of the target integration site. The integration cassette, conceptually similar to those used to target integration of vectors described here, can easily be constructed in a single step, for instance using InFusion or overlapping PCR, and integrated in the pFA6a vector series. In conclusion, SIV plasmids add to the existing panel of tools available to fission yeast researchers.

Plasmid modularity and versatility

Because every experimental design is different and there is no single vector that can fit all needs, the vector series presented here has been developed with modularity in mind. Simple subcloning can easily re-target a construct to a different genomic locus, introduce a different selection marker, exchange the fluorescent tag or alter the level of expression. We already generated a set of highly used cell biology markers that can be combined through genetic crosses and are predominantly away from the most frequently targeted *ura4* locus. These can also be targeted to different loci or in other colour, at will. We encourage the further expansion of the SIV series through introduction for instance of additional tags or inducible promoters (Kjaerulff and Nielsen, 2015; Ohira et al., 2017; Zilio et al., 2012).

The design choice will be dictated by the experiment (see section on 'Recommendations for use of the vectors' below for recommendation on experimental design and plasmid use). For instance, while selecting for prototrophs is more cost effective, this requires transformation into an auxotrophic strain. For this, both strains carrying point mutations, which are present in most strain collections, and the new deletion alleles we constructed (*ade6-D19*, *lys3-D20* and *his5-D21*; Figs 1F,G and 2C,D), as well as the previously described *ura4-D18* allele (Grimm et al., 1988), are suitable. However, we find that prototrophic restoration of the selective marker without integration of the accompanying vector sequences occurs in up to 8% of the total transformants when using point mutants (Figs 1F,G and 2C,D). Thus, strains with deletion alleles should be used when it is important to avoid false-positive transformants. For example, high rates of false-positive transformants may make it complicated to quantify how introducing genes of interest affects the capacity of cells to form colonies (Li and McLeod, 1996). High rates of false-positive transformants may also increase the aworkload when screening transformants obtained using a plasmid library. Using deletion alleles in the parental strain precludes homologous recombination of the selective marker alone, but we note that unintended transformant genotypes may still rarely arise when integration is achieved by non-homologous repair (Chang et al., 2017; Fennessy et al., 2014). The vector variants containing an antibiotic selection marker (Fig. 3A) should also exhibit low false-positive rates when selecting for the antibiotic resistance but not when selecting for prototrophic transformants. The plethora of dominant antibiotic resistance markers is particularly useful since vectors can be directly integrated into most genetic backgrounds without the need for a pre-existing auxotrophy. The limit would only be reached in prototrophs already containing the five different antibiotic resistances used here.

The series of the promoters we provide induces expression levels that span more than three orders of magnitude and thus should accommodate a wide range of applications. We note that, for the same promoter, we did not observe changes in expression levels between different genomic loci (Fig. 3C,D). However, we refrain from using different constructs to compare between conditions as genomic position effects may become evident only in certain backgrounds (Allshire and Ekwall, 2015). While we present the full vector series for the first time here, some plasmids have been used in published studies (Billault-Chaumartin and Martin, 2019; Gerganova et al., 2019; Lamas et al., 2019 preprint; Marek et al., 2019 preprint; Vještica et al., 2018), which illustrates their application in fission yeast research.

Recommendations for use of the vectors

For best use of the tools described here, we make a few recommendations as follows:

1. Clone your construct in your plasmid of choice according to experimental design, bearing in mind that the restriction enzyme used for linearization (*AfeI*, *PmeI*, *BstZ17I* or *StuI* in pUra4^{AfeI}, pAde6^{PmeI}, pLys3^{BstZ17I} and pHis5^{StuI}, respectively) should remain unique after cloning.
    - In some cases, combinations of other restriction enzymes can be used for linearization as long as they produce a single linear fragment with two large homology arms (e.g. *RsrII* and *BlpI* can be used together on pAde6^{PmeI});
    - Bear in mind that the multiple cloning sites between plasmids of the same sets are identical but not all restriction enzymes are unique in all cases. While plasmids carrying the antibiotic-resistance markers are designed to receive constructs from other plasmids by *Sac*I-*Kpn*I digestion, antibiotic markers can also be shuttled into the promoter series by using a unique site in either the *ColE1* or *AmpR* genes and *SacI* or *BglII*;
    - Blunt restriction enzyme sites (e.g. *Pml*I, *Sma*I, *Swa*I) have been introduced in some of the plasmids to increase their modularity. Similarly, restriction sites that use compatible cohesive ends (e.g. *XhoI-SalI* pair) increase the ability to shift constructs between plasmids;
    - In our experience, a single ligation reaction can readily combine three elements into a single plasmid (e.g. p^{act1} cut with *Kpn*I and *Eco*RI from pAV0714, mTagBFP2 cut with *Eco*RI and *Asc*I from pAV0471 and the vector sequences from pAV0783 cut with *Kpn*I and *Asc*I);
    - Other protein tags can be cloned in place of the sfGFP sequence, preserving the STOP codon in the MCS after the tag, to allow for both N- and C-terminal tagging;
    - In addition to the main 22 plasmids discussed in the text, we also provide 22 plasmids that were used in building the strains presented in Fig. 4. These include additional promoters (e.g. *the constitutive promoter* p^{atb2} and p^{bip1}, and the mating type-specific promoters p^{mam1*} and p^{map3}), fluorophores (e.g. 3GFP, 3mCherry, 3mTagBFP2) and a terminator (*S. cerevisiae ADH1*) that may be better suited for some uses.
2. Linearize 700 µg of the plasmid and transform in the strain, using either prototrophy or antibiotic selection;
3. Verify correct integration by diagnostic PCRs on both sides of the integration sites with primers as described in Fig. S1.

Journal of Cell Science (2020) 133, jcs240754. doi:10.1242/jcs.240754

MATERIALS AND METHODS

Plasmids

All plasmids were generated using standard restriction enzyme cloning and InFusion system (TaKaRa Bio, Kusatsu, Japan). The list of all plasmids used in the study is available in Table S1. Annotated GenBank format sequences for all constructs used in the study are available from Figshare (https://doi.org/10.6084/m9.figshare.10689188.v1, source data D1). Plasmids that are of general use are available from Addgene (Watertown, USA; https://www.addgene.org) and the Japanese National BioResource Project (NBRP, Osaka, Japan; http://yeast.nig.ac.jp). All plasmids used to test the system, which are derivatives of the ones available from these resource centers, are available from the Martin laboratory upon reasonable request.

The plasmid backbones were amplified from pJK210 which itself was derived from pBluescript SK (+) and encode for ColE1 and F1 replication origins, ampicillin selection cassette, a multiple cloning site and T3, T7 and M13 primer sequences. Dominant selection markers kanMX6, natMX6, hphMX6, bleMX6 for yeast selection were amplified from the pFA6a vector series (Bähler et al., 1998; Hentges et al., 2005; Wach et al., 1994). The bsdMX6 selection marker was amplified from the fission yeast strain VS6381, a kind gift from Viesturs Simanis (EPFL, Switzerland) and Masamitsu Sato (Waseda University, Japan). We noticed sequence variation in comparison to original sequences, but report that all markers were fully functional. All fission yeast sequences were amplified from the genomes of wild-type strains 968 (ySM1396), 972 (ySM995) or 975 (ySM1371).

For promoter sequences, we used the sequences immediately upstream of the START codon. Promoter p^{tdh1} contains 1000 bp, while p^{tdh1*} contains 896 bp (used only in pAV0471, pAV0765, pAV0532 and pAV0569–pAV0572). p^{act1} includes 822 bp, p^{rga3} includes 1203 bp, p^{pom1} includes 688 bp, p^{map3} includes 2063 bp, p^{atb2} includes 647 bp, p^{bip1} includes 988 bp, p^{pcn1} includes 1954 bp, p^{pak1} includes 630 bp, p^{urg1} includes 675 bp and p^{nmt1} includes 1177 bp. The p^{nmt41} and p^{nmt81} promoters were obtained by subsequently mutating the p^{nmt1} using nested PCR (with mutations as reported in Basi et al., 1993). p^{mam1*} includes 1751 bp and was point mutated to remove the *Afe*I site.

For terminator sequences, we used the sequences immediately after the STOP codon of *Saccharomyces cerevisiae* genes *ADH1* (229 bp) and *CYC1* (250 bp). We also used the 988 bp downstream of the fission yeast *nmt1* gene STOP codon. In case of sequences designated as the *tdh1* terminator, we used a fragment containing the sequence between STOP+332 bp and STOP+1032 bp. We note that this fragment does not include the 3′UTR sequence of the *tdh1* gene but led to a notable increase in protein levels as compared to constructs lacking any terminator sequence.

Fluorescent protein sequences were obtained from laboratory stocks with the exception of mTagBFP2 which was amplified from mTagBFP2-pBAD (Addgene #54572). The 3mTagBFP2 was a kind gift from Serge Pelet (University of Lausanne, Switzerland).

All the probes are derived from previous publications. The RitC amphipathic helix encodes the 62 C-terminal amino acids from the mammalian Rit protein (Onken et al., 2006). The nuclear localization signal uses the viral SV40 motif (PKKKRKV, Kalderon et al., 1984). Nuclear export signals were derived from fission yeast genes Mia1/Alp7 (EDLVIAMDQLNLEQ, Ling et al., 2009) and Wis1 (QPLSCSLRQLSISP, Nguyen et al., 2002). The CRIB probe encodes amino acids 2–181 from *S. cerevisiae* protein Gic2, in contrast to CRIB construct used by Tatebe et al. (2008) which used amino acids 1–208. The RasAct probe encodes Byr1 amino acids 65–180 in three tandem repeats (Merlini et al., 2018). The LifeAct probe encodes a MGVADLIKKFESISKE peptide (Riedl et al., 2008). The CHD probe contains amino acids 1–189 from the Rng2 protein (Wang et al., 2004). The N-terminal signal sequence comprising amino acids 1–25 from the BiP (Bip1) protein targets the fluorophore to the ER while the C-terminal ADEL motif ensures its retention in the ER (Zhang et al., 2010). Microtubules are visualized by use of full-length Atb2 (Cassimeris and Tran, 2010) and replication sites by use of Pcn1 (Meister et al., 2007), both tagged at the N-terminus and expressed as a second copy.

Growth conditions

Yeast cells were grown in standard fission yeast medium at either 25°C or 30°C (Hagan, 2016) and using 200 rpm rotators for liquid media. For genetic manipulations we used YES medium. For selection we supplemented YES with 100 µg/ml G418/kanamycin (cat. no. G4185, Formedium, Norfolk, UK), 100 µg/ml nourseothricin (HKI, Jena, Germany), 50 µg/ml hygromycinB (cat. no.10687010, Invitrogen), 100 µg/ml zeocin (cat. no. R25001, Thermo Fisher Scientific), and 15 µg/ml blasticidin-S (cat. no. R21001, Thermo Fisher Scientific). 5-FOA (cat. no. 003234, Fluorochem, Derbyshire, UK) was used at 1 mg/ml in Edinburgh minimal medium (EMM) supplemented with 50.25 µg/ml uracil (U0750-100G, Sigma-Aldrich, St Louis, MO). For western blotting, flow cytometry and imaging, we used EMM-ALU medium, which is EMM medium supplemented with 255 µg/ml adenine hemisulfate (A9126-100G, Sigma-Aldrich), 255 µg/ml leucine (L8000-100G, Sigma-Aldrich) and 255 µg/ml uracil (U0750-100G, Sigma-Aldrich). Briefly, cells were precultured overnight in liquid EMM-ALU and then again sub-cultured overnight to reach the exponential phase. Repression of the *nmt* promoters was achieved by supplementing thiamine at final concentration of 5 µg/ml. Activation of the *nmt* promoters was achieved by washing out thiamine and growing cells for minimum of 24 h. The *urg1* promoter was induced by addition of uracil at final concentration 250 µg/ml for at least 48 h. Conditions used to mate cells are detailed in Vjestica et al. (2016). Briefly, cells were precultured overnight in MSL+N media and then sub-cultured overnight to reach the exponential phase. Cells of opposite mating types were then mixed in equal amounts, washed three times and resuspended in MSL-N to give a final OD_{600nm}=1.5 and incubated at 30°C with 200 rpm agitation for 4–6 h prior to mounting for imaging.

Yeast strains

The list of all strains used in the study is available in Table S2. Strains of general use are available from the Japanese National BioResource Project (NBRP, Osaka, Japan; http://yeast.nig.ac.jp).

All fission yeast strains were obtained by standard lithium acetate transformation protocol (Hagan, 2016). We used ∼700 ng of the linearized plasmid per transformation. Unless otherwise indicated, plasmids were linearized with a single restriction enzyme present in between the two homology regions (e.g. *Afe*I for pUra4^{AfeI}). In some instances, subcloned constructs contained an additional cutting site for the enzyme normally used to linearize the vector. As indicated in the yeast strain table (Table S2), we overcame this problem by using two enzymes that flank the regular linearization sites (e.g. *Rsr*II and *Blp*I for pAV0782) which leads to slightly shorter homology arms. This did not affect the ability to obtain correct transformants.

The *ura4-294*, *ade6-M210*, *lys3-37* are commonly used *S. pombe* point mutant strains that are available in many lab stocks. The *his5Δ1* strain was obtained from Dr Mohan Balasubramanian (Warwick Medical School, University of Warwick, UK) (Tang et al., 2011). *ade6-M210* carries a C1466T substitution, whereas the exact mutations of other alleles are not known. The auxotrophic *ura4-D18* mutation (Grimm et al., 1988), which lacks the 1.8 kb *Hind*III fragment flanking the ura4 ORF, was obtained by crossing out from the Martin group yeast library (YSM1131). To generate auxotrophic *ade6-D19*, *lys3-D20* and *his5-D21* deletions, we first inserted the *ura4+* selection cassette into the pAde6^{PmeI}, pLys3^{BstZ17I} and pHis5^{StuI} vector to obtain plasmids pAV0596, pAV0597 and pAV0598. The resulting plasmids were linearized to target their integration at the *ade6*, *lys3* and *his5* genomic loci, respectively. Each linearized plasmid was separately transformed into the yeast strain carrying the *ura4-D18* mutation. Selection for uracil prototrophy yielded strains where a functional *ura4+* cassette was now linked with either *ade6*, *lys3* or *his5* locus, while the native *ura4* locus carried the *ura4-D18* mutation. These strains were then transformed with DNA fragments spanning both sides of the *ura4+* integration site and carrying the *ade6-D19*, *lys3-D20* or *his5-D21* deletions (see Supplemental Sequences). Recombinants that remove the *ura4+* cassette and replace the locus with the deletion allele were selected on 5-FOA. The *ade6-D19* allele is lacking the fragment from STOP−776 bp to STOP+159 bp, the *lys3-D20* allele lacks sequences between STOP−895 bp and STOP+367 bp, and the *his5-D21* allele lacks the fragment from STOP−524 bp to STOP+378 bp. The correct transformants were confirmed by diagnostic PCRs (the PCR-PΔ indicated in the Fig. S1) and then backcrossed six times with the wild-type fission yeast strain 975 (YSM1371) to obtain the final strains. The *h90* strains were obtained through crosses with wild-type fission yeast strain 968 (YSM1396).

All other strains were obtained by transforming linearized plasmids into either auxotrophic strains and selecting for prototrophs, or into prototrophs

Journal of Cell Science (2020) 133, jcs240754. doi:10.1242/jcs.240754

and selecting for antibiotic resistance. Multiple transformants were genotyped to verify correct plasmid integration. Since expression levels between several transformants did not vary, we assumed that they all carried a single integrated copy.

gDNA extraction

Genomic (g)DNA was extracted using a protocol described by Lõoke et al. (2011) with minor modifications. Briefly, ∼5×10^7 of freshly streaked cells was resuspended in 100 µl of the isolation buffer (250 mM lithium acetate and 1% SDS) in a microfuge tube. Samples were incubated for 10 min at 70°C and briefly vortexed. We added 300 µl of 100% ethanol to each sample and briefly vortexed. Next, we spun down the samples at 15,000 ***g*** for 3 min. The pellet was washed with 70% ethanol twice. The pellet was briefly dried to remove traces of ethanol. We then dissolved the pellet in 100 µl of 5 mM Tris-HCl and spun down the cell debris for 1 min at 3000 ***g***. The supernatant was transferred to a fresh tube and the concentration was adjusted to 100 µg/ml. The samples were used for both standard and quantitative PCR amplifications.

Genotyping

An overview of the diagnostic PCR reactions used to confirm genomic integration of the vector at the desired locus is presented in Fig. S1. Sequences of the primers used are available in Table S3. Briefly, we tested recombination for each homology arm of the vectors by PCRs with one vector-specific and one genome-specific oligonucleotide (Fig. S1, right panel). Simultaneously we tested for the presence of the parental locus using two genome-specific oligonucleotides. We used different primers to test the prototrophic and auxotrophic parental loci. Only transformants where all three PCRs indicated correct integration were used further.

Standard PCRs were performed with 5 µM primers, 5 ng/µl of the gDNA and a polymerase made in-house using the following cycler program:

$$\frac{98°C}{150\,s} \rightarrow 30 \times \left[\frac{98°C}{20\,s} \rightarrow \frac{54°C}{30\,s} \rightarrow \frac{72°C}{90\,s}\right] \rightarrow \frac{72°C}{600\,s}.$$

The *ade6* PCR-U (Fig. S1) was performed with commercial Kapa-Taq (Kapa Biosystems, Wilmington, NC) and the PCR program:

$$\frac{96°C}{150\,s} \rightarrow 35 \times \left[\frac{96°C}{30\,s} \rightarrow \frac{51°C}{30\,s} \rightarrow \frac{72°C}{180\,s}\right] \rightarrow \frac{72°C}{600\,s}.$$

Quantitative PCR

We used qPCR to monitor the number of plasmid integration events into the genome. The raw EDS format data (Source Data D2) and processed results (Source Data D3) are available from Figshare (https://doi.org/10.6084/m9.figshare.10689188.v1). Experiments were performed on the QuantStudio™5 (Applied Biosystems) using SYBR Select Master Mix (Applied Biosystems; cat. no. 4472908) and primers at a final concentration of 0.2 µM. The final reaction volume was 10 µl. Each biological sample was evaluated in a technical triplicate. Technical outliers were rare and were not removed. Each experiment included a negative control (water), which did not show any considerable signal amplification. An identical detection threshold of fluorescence intensity was set for all targets and all qPCR samples in the study, and used to determine the cycle threshold (Ct) value. We monitored amplification of a *ura4* 142 bp fragment using primers osm6182 (5′-GGC-TGGGACAGCAATATCGT-3′) and osm6183 (5′-GCCTTCCAACCAGC-TTCTCT-3′) and *act1* 149 bp fragment using primers osm6178 (5′-GTGTTACCCACACTGTTCCCA-3′) and osm6179 (5′-TTCACGTTCGG-CGGTAGTAG-3′). We first amplified the 10-fold dilution series of wild-type genomic DNA (extraction protocol as detailed above) at final concentrations in the range 0.01–100 ng/µl, which established primer efficiencies of 1.99 (R2=0.998) and 2.04 (R2=0.999) and intercepts of 18.53 and 19.06 for *ura4* and *act1* primer pairs, respectively. In subsequent experiments, we used genomic DNA at a final concentration of 10 ng/µl and the formula:

$$\frac{[ura4]}{[act1]} = \frac{1.99^{18.53-Ct_{ura4}}}{2.04^{19.06-Ct_{act1}}}$$

to compare relative levels of *ura4* and *act1* loci. We proceeded to show that we can reproducibly detect a relative increase in *ura4* locus copy number by using strains that carry one (ySM1371: *wt, ura4+*), two (AV0138: *pak2Δ:ura4+ ura4+*) and three (AV0226: *myo52Δ:ura4+ pak2Δ:ura4+ ura4+*) copies of the *ura4* locus but only one *act1* locus. All subsequent experiments included each of these samples as positive controls.

To quantify the number of integrated copies of the vectors pJK210 and pUra4^{AfeI} we transformed the linearized vectors into *ura4-294* and *ura4-D18* auxotrophic strains, respectively, and extracted the genomic DNA from 12 prototrophic transformants. qPCR analysis of relative *ura4* and *act1* loci abundance was used to determine the number of integration events. For vectors pAde6^{PmeI}, pLys3^{BstZ17I} and pHis5^{StuI}, we first introduced the *ura4* cassette to produce plasmids pAV0596, pAV0597 and pAV0597. Linearized vectors were transformed into *ade6-D19 ura4-D18*, *lys3-D20 ura4-D18* or *his5-D21 ura4-D18* double mutants, respectively, and selected for uracil prototrophy. A total of 12 transformants from each transformation were then used to extract gDNA, establish relative levels of *act1* and *ura4* loci, and determine the number of integration events.

Quantification of false-positive integrants and transformation efficiencies

To measure the proportion of false-positive integrations, we introduced sfGFP under the strong *tdh1* promoter into pUra4^{AfeI}, pAde6^{PmeI}, pLys3^{BstZ17I} and pHis5^{StuI} plasmids, which resulted in plasmids pAV0569, pAV0570, pAV0571 and pAV0572. After linearization, the plasmids were transformed into adequate auxotrophic strains and plated on media selecting for prototrophy. The transformation efficiency was calculated as the proportion of cells that formed colonies from the total number of cells that was transformed. Once colonies formed, we imaged the selective plates using Fusion FX (Vilber, Collégien, France). While white light was used to observe all clones, we detect the green fluorescent protein using the 480 nm LED illumination and the F535Y filter (535/50). This allowed us to distinguish between fluorescent and non-fluorescent clones. The percentage of non-fluorescent colonies was used as a measure of false-positive transformants. We report the mean±s.d. of three independent experiments. We also report the *P*-values from the paired Student's *t*-test.

Quantification of stability of loci generated by plasmid integration

To quantify the stability of loci generated by integration of pJK210 and pUra4^{AfeI} plasmids, we exploited the 5-FOA counter-selection against *ura4+*. First, we cloned the natMX6 cassette into the two vectors to obtain plasmids pAV0584 and pAV0623. The resulting plasmids were linearized, transformed into cells carrying the *ura4-294* point mutation and, for each transformation, six nourseothricin-resistant uracil prototrophs were selected. To reveal any instability in the introduced loci, we grew the 12 transformants, and an additional four clones of the wild-type prototrophic strain, as a negative control, on non-selective (uracil supplemented, no nourseothricin) medium for 3 days. The strains were first passaged twice on non-selective solid medium over 2 days. We then precultured each clone in non-selective, liquid medium overnight to exponential phase and plated 1.4×10^7 cells onto 5-FOA medium containing uracil, which selects for *ura4−* cells. 5-FOA-resistant clones were replica plated onto medium containing nourseothricin to check whether the entire locus was lost. We report the average proportion of 5-FOA-resistant clones out of 1.4×10^7 cells that we plated, and the percentage of those that retained the nourseothricin-resistance marker. Significance was determined using the Kruskal–Wallis test.

Since drugs to counter-select against *ade6+*, *lys3+* and *his5+* were not available, we introduced both the *ura4+* and an antibiotic cassette into pAde6^{PmeI}, pLys3^{BstZ17I} and pHis5^{StuI} plasmids, which resulted in plasmids pAV0616, pAV0617 and pAV0618. This allowed us to use the same strategy as above to quantify the stability of loci generated by our vector series, the only difference being that we performed it using four and not six initial transformants. Significance was determined using the Kruskal–Wallis test.

Microscopy and image quantification

All images shown in Fig. 4 were obtained by wide-field microscopy performed on a DeltaVision platform (Applied Precision) composed of a customized inverted microscope (IX-71; Olympus), a UPlan Apochromat 100×/1.4 NA or 60×/1.4 NA oil objective, a camera (CoolSNAP HQ2; Photometrics), and a color combined unit illuminator (Insight SSI 7; Social Science Insights). Images were acquired using softWoRx v4.1.2 software (Applied Precision). The mTagBFP2 was imaged using the DAPI/FITC/TRITC/CY5™ filterset which allows bandpass excitation (390/18) and emission (435/48). We used the GFP-mCherry™ filterset to detect the green (excitation 475/28, emission 525/50) and red (excitation 575/25; emission 632/60) fluorescent proteins. We imaged a different number of *Z*-sections to best capture the structure of interest. We present either a single *Z*-plane or a projection image. All image processing was performed using standard ImageJ/Fiji (NIH, Bethesda, USA) built-in modules, except for images where deconvolution was performed using the softWoRx v4.1.2 built-in module.

To quantify relative promoter strengths, we imaged cells expressing sfGFP from the indicated promoters, using a spinning disk confocal setup comprising a DMI4000B inverted microscope equipped with an 100× HCX PL APO 6100 (NA 1.46) oil objective and Perkin-Elmer Confocal system (including a Yokagawa CSU22 real-time confocal scanning head and solid-state laser lines). *Z*-series of confocal sections were acquired at 0.4 µm intervals using the Volocity software.

For quantifications, we prepared an average projection image of three medial *Z*-sections. Next, we outlined the cell boundaries and measured the mean fluorescence intensity of at least 25 untagged wild-type cells and 25 cells expressing cytosolic sfGFP from the indicated promoters. Next, we subtracted the mean fluorescence of wild-type cells from each cell carrying the sfGFP gene that was imaged in identical conditions. We then calculated the mean intensity and standard deviation for cells of the same genotype. Since sfGFP expression levels induced by different promoters varied by more than three orders of magnitude, the samples imaged under the same imaging conditions were standardized to the signal from $ura4^{+}$:p^{act1}:*sfGFP* cells, which was set to 100 arbitrary units. The data presented is the mean intensity, and standard deviation is denoted.

For images in Fig. 4, we concentrated exponentially growing cells by centrifugation at 1000 ***g*** and spotted them directly between slide and coverslip for immediate imaging. For images in Fig. 3 and time-lapse imaging, we placed cells in chambers with solid medium made with 2% agarose, as previously described (Vjestica et al., 2016).

Western blotting and protein level quantification

We grew 70 ml of each strain in EMM, supplemented with 5 µg/ml of thiamine or 50.25 µg/ml of uracil as indicated, to exponential phase and collected cells by centrifugation for 5 min at 1000 ***g***. Samples were frozen in liquid nitrogen and stored at −80°C until ready for processing. Subsequent steps were performed at 4°C. Samples were thawed and transferred into 2 ml microcentrifuge tubes, washed twice with ice-cold PBS buffer (137 mM NaCl, 2.7 mM KCl, 10 mM Na2HPO$_4$, 1.8 mM KH$_2$PO$_4$, pH 7.5, and protease inhibitor mix) and re-suspended in 500 µl of the PBS buffer. ∼1 ml of acid-washed glass beads were added. Cells were lysed using the FastPrep-24 bead-beater (MP Biomedicals, Santa Ana, CA) set to 4.5 m/s with 10 cycles of 20 s beating and 40 s cooling on ice. We then pierced the bottom of the tube with a heated needle, placed that tube into a 1.5 ml microfuge tube and centrifuged it at 150 ***g*** for 60 s. In this manner, we discarded the beads and transferred the samples to a new tube. Cell debris was pelleted by centrifugation for 15 min at 13,000 ***g***. We collected the supernatant and determined the protein concentration using the Bradford assay. All samples were adjusted to the same protein concentration and re-suspended in Laemmli buffer, heated to 90°C for 5 min and then subjected to SDS-PAGE (XP10205BOX, Thermo Fisher Scientific). The gel was then blotted onto nitrocellulose membrane using the Towbin transfer buffer (25 mM Tris base, 192 mM glycin, 20% methanol, pH 8.3). After blocking in 5% milk, the membrane was first probed with an anti-GFP antibody (cat. no. 11814460001, Roche, Basel, Switzerland; 1:3000 dilution) followed by a secondary anti-mouse-IR800 (R-05061, Advansta, Menlo Park, CA), and visualized on the Fusion FX (Vilber, Collégien, France). Subsequently, the same membrane was probed with the anti-TAT-1 antibody (a kind gift from Keith Gull, University of Oxford, UK; used at 1:3000 dilution) targeting tubulin as a loading control. We used ImageJ/Fiji to quantify the signal detected for GFP and normalized it to the tubulin signal. We used the unlabelled area of the membrane as the background intensities. The experiment was qualitatively reproduced in two independent replicates and results quantified from the second replicate.

Flow cytometry

Flow cytometry was performed on a BD Biosciences Fortessa analyser using CellQuest software. To stain for dead cells in the population, cells were diluted in EMM-ALU medium to final OD_{600} 0.4 and 100 µl of cell suspension was mixed with 900 µl EMM-ALU medium containing 1 µg/ml propidium iodide (PI). After 30 s of incubation cells were analysed by flow cytometry without gating during acquisition with 10^4 cells recorded for each sample. Data were analysed using the FlowJo software package using the following gating strategy: (1) the main cellular population was distinguished using forward and side scatter to exclude cell aggregates, (2) doublets were excluded from analysis by plotting FSC-A versus FSC-H and gating along the diagonal, (3) dead cells were excluded from analysis by gating out PI-positive events, and (4) GFP-positive events were detected in the green channel. More than 70% of all events passed the indicated criteria.

Statistical analysis

Statistical tests used were the Kruskal–Wallis or Student's *t*-test, as described above. Sample sizes were not pre-determined. No sample was excluded. No randomization or blinding was used.

Acknowledgements

We are grateful to Lucie Kesnerova and Philip Engel for help with the qPCR experiments, Serge Pelet (Department of Fundamental Microbiology, University of Lausanne, Switzerland) for the gift of the 3mTagBFP2 construct, Viesturs Simanis (Swiss Federal Institute of Technology EPFL, Switzerland) for the gift of the bsdMX6-containing strain and Masamitsu Sato (Faculty of Science and Engineering, Waseda University, Japan) for the bsdMX6 sequence.

Competing interests

The authors declare no competing or financial interests.

Author contributions

Conceptualization: A.V.; Methodology: A.V., M.M.; Formal analysis: A.V., M.M.; Investigation: A.V., M.M., P.J.N., L.M., G.L., M.B., I.B.-C.; Writing - original draft: A.V., M.M.; Writing - review & editing: A.V., M.M., S.G.M.; Supervision: S.G.M.; Project administration: S.G.M.; Funding acquisition: S.G.M.

Funding

This work was funded by a European Research Council (ERC) Consolidator Grant (CellFusion) and a Schweizerischer Nationalfonds zur Förderung der Wissenschaftlichen Forschung (Swiss National Science Foundation) grant (310030B_176396) to S.G.M.

Data availability

Annotated GenBank format sequences for all constructs used in the study source data D1, as well as the raw qPCR EDS format data (source data D2) and processed results (source data D3) are available from Figshare (https://doi.org/10.6084/m9.figshare.10689188.v1).

Supplementary information

Supplementary information available online at
http://jcs.biologists.org/lookup/doi/10.1242/jcs.240754.supplemental

Peer review history

The peer review history is available online at
https://jcs.biologists.org/lookup/doi/10.1242/jcs.240754.reviewer-comments.pdf

References

Alam, M. T., Zelezniak, A., Mülleder, M., Shliaha, P., Schwarz, R., Capuano, F., Vowinckel, J., Radmaneshfar, E., Krüger, A., Calvani, E. et al. (2016). The metabolic background is a global player in Saccharomyces gene expression epistasis. *Nat. Microbiol.* **1**, 15030. doi:10.1038/nmicrobiol.2015.30

Allshire, R. C. and Ekwall, K. (2015). Epigenetic regulation of chromatin states in Schizosaccharomyces pombe. *Cold Spring Harb. Perspect. Biol.* **7**, a018770. doi:10.1101/cshperspect.a018770

Bähler, J., Wu, J.-Q., Longtine, M. S., Shah, N. G., McKenzie, A., III, Steever, A. B., Wach, A., Philippsen, P. and Pringle, J. R. (1998). Heterologous modules for efficient and versatile PCR-based gene targeting in Schizosaccharomyces pombe. *Yeast* **14**, 943-951. doi:10.1002/(SICI)1097-0061(199807)14:10<943::AID-YEA292>3.0.CO;2-Y

Basi, G., Schmid, E. and Maundrell, K. (1993). TATA box mutations in the Schizosaccharomyces pombe nmt1 promoter affect transcription efficiency but not the transcription start point or thiamine repressibility. *Gene* **123**, 131-136. doi:10.1016/0378-1119(93)90552-E

Billault-Chaumartin, I. and Martin, S. G. (2019). Capping protein insulates Arp2/3-assembled actin patches from formins. *Curr. Biol.* **29**, 3165-3176.e6. doi:10.1016/j.cub.2019.07.088

Cassimeris, L. and Tran, P. (2010). *Microtubules: In Vivo*. 1st edn. Amsterdam; Boston, MA: Elsevier/Academic Press.

Chan, K.-M., Liu, Y.-T., Ma, C.-H., Jayaram, M. and Sau, S. (2013). The 2 micron plasmid of Saccharomyces cerevisiae: a miniaturized selfish genome with optimized functional competence. *Plasmid* **70**, 2-17. doi:10.1016/j.plasmid.2013.03.001

Chang, H. H. Y., Pannunzio, N. R., Adachi, N. and Lieber, M. R. (2017). Non-homologous DNA end joining and alternative pathways to double-strand break repair. *Nat. Rev. Mol. Cell Biol.* **18**, 495-506. doi:10.1038/nrm.2017.48

Chen, Y.-H., Wang, G.-Y., Hao, H.-C., Chao, C.-J., Wang, Y. and Jin, Q.-W. (2017). Facile manipulation of protein localization in fission yeast through binding of GFP-binding protein to GFP. *J. Cell Sci.* **130**, 1003-1015. doi:10.1242/jcs.198457

Clarke, L. (1990). Centromeres of budding and fission yeasts. *Trends Genet.* **6**, 150-154. doi:10.1016/0168-9525(90)90149-Z

Clarke, L. and Carbon, J. (1980). Isolation of a yeast centromere and construction of functional small circular chromosomes. *Nature* **287**, 504-509. doi:10.1038/287504a0

Craven, R. A., Griffiths, D. J. F., Sheldrick, K. S., Randall, R. E., Hagan, I. M. and Carr, A. M. (1998). Vectors for the expression of tagged proteins in Schizosaccharomyces pombe. *Gene* **221**, 59-68. doi:10.1016/S0378-1119(98)00434-X

Farlow, A., Long, H., Arnoux, S., Sung, W., Doak, T. G., Nordborg, M. and Lynch, M. (2015). The spontaneous mutation rate in the fission yeast Schizosaccharomyces pombe. *Genetics* **201**, 737-744. doi:10.1534/genetics.115.177329

Fennessy, D., Grallert, A., Krapp, A., Cokoja, A., Bridge, A. J., Petersen, J., Patel, A., Tallada, V. A., Boke, E., Hodgson, B. et al. (2014). Extending the Schizosaccharomyces pombe molecular genetic toolbox. *PLoS ONE* **9**, e97683. doi:10.1371/journal.pone.0097683

Forsburg, S. L. and Sherman, D. A. (1997). General purpose tagging vectors for fission yeast. *Gene* **191**, 191-195. doi:10.1016/S0378-1119(97)00058-9

Gadaleta, M. C., Iwasaki, O., Noguchi, C., Noma, K.-I. and Noguchi, E. (2013). New vectors for epitope tagging and gene disruption in Schizosaccharomyces pombe. *BioTechniques* **55**, 257-263. doi:10.2144/000114100

Gerganova, V., Floderer, C., Archetti, A., Michon, L., Carlini, L., Reichler, T., Manley, S. and Martin, S. G. (2019). Multi-phosphorylation reaction and clustering tune Pom1 gradient mid-cell levels according to cell size. *eLife* **8**, e45983. doi:10.7554/eLife.45983

Grimm, C., Kohli, J., Murray, J. and Maundrell, K. (1988). Genetic engineering of Schizosaccharomyces pombe: a system for gene disruption and replacement using the ura4 gene as a selectable marker. *Mol. Gen. Genet.* **215**, 81-86. doi:10.1007/BF00331307

Hachet, O., Berthelot-Grosjean, M., Kokkoris, K., Vincenzetti, V., Moosbrugger, J. and Martin, S. G. (2011). A phosphorylation cycle shapes gradients of the DYRK family kinase pom1 at the plasma membrane. *Cell* **145**, 1116-1128. doi:10.1016/j.cell.2011.05.014

Hagan, I. (2016). *Fission Yeast: A Laboratory Manual* (ed. I. Hagan). Cold Spring Harbor Laboratory Press.

Hentges, P., Van Driessche, B., Tafforeau, L., Vandenhaute, J. and Carr, A. M. (2005). Three novel antibiotic marker cassettes for gene disruption and marker switching inSchizosaccharomyces pombe. *Yeast* **22**, 1013-1019. doi:10.1002/yea.1291

Hoffman, C. S., Wood, V. and Fantes, P. A. (2015). An ancient yeast for young geneticists: a primer on the Schizosaccharomyces pombe model system. *Genetics* **201**, 403-423. doi:10.1534/genetics.115.181503

Jasin, M. and Rothstein, R. (2013). Repair of strand breaks by homologous recombination. *Cold Spring Harb. Perspect. Biol.* **5**, a012740. doi:10.1101/cshperspect.a012740

Kakui, Y., Sunaga, T., Arai, K., Dodgson, J., Ji, L., Csikász-Nagy, A., Carazo-Salas, R. and Sato, M. (2015). Module-based construction of plasmids for chromosomal integration of the fission yeast Schizosaccharomyces pombe. *Open Biol.* **5**, 150054. doi:10.1098/rsob.150054

Kalderon, D., Roberts, B. L., Richardson, W. D. and Smith, A. E. (1984). A short amino acid sequence able to specify nuclear location. *Cell* **39**, 499-509. doi:10.1016/0092-8674(84)90457-4

Keeney, J. B. and Boeke, J. D. (1994). Efficient targeted integration at leu1-32 and ura4-294 in Schizosaccharomyces pombe. *Genetics* **136**, 849-856.

Kimura, M., Takatsuki, A. and Yamaguchi, I. (1994). Blasticidin S deaminase gene from Aspergillus terreus (BSD): a new drug resistance gene for transfection of mammalian cells. *Biochim. Biophys. Acta Gene Struct. Expr.* **1219**, 653-659. doi:10.1016/0167-4781(94)90224-0

Kjaerulff, S. and Nielsen, O. (2015). An IPTG-inducible derivative of the fission yeast nmt promoter. *Yeast* **32**, 469-478. doi:10.1002/yea.3073

Lamas, I., Merlini, L., Vještica, A., Vincenzetti, V. and Martin, S. G. (2019). Optogenetics reveals Cdc42 local activation by scaffold-mediated positive feedback and Ras GTPase. *bioRxiv*, 710855. doi:10.1101/710855

Lee, A. H., Symington, L. S. and Fidock, D. A. (2014). DNA repair mechanisms and their biological roles in the malaria parasite plasmodium falciparum. *Microbiol. Mol. Biol. Rev.* **78**, 469-486. doi:10.1128/MMBR.00059-13

Li, P. and McLeod, M. (1996). Molecular mimicry in development: identification of ste11+ as a substrate and mei3+ as a pseudosubstrate inhibitor of ran1+ kinase. *Cell* **87**, 869-880. doi:10.1016/S0092-8674(00)81994-7

Ling, Y. C., Vjestica, A. and Oliferenko, S. (2009). Nucleocytoplasmic shuttling of the TACC protein Mia1p/Alp7p is required for remodeling of microtubule arrays during the cell cycle. *PLoS ONE* **4**, e6255. doi:10.1371/journal.pone.0006255

Lõoke, M., Kristjuhan, K. and Kristjuhan, A. (2011). Extraction of genomic DNA from yeasts for PCR-based applications. *BioTechniques* **50**, 325-328. doi:10.2144/000113672

Marek, M., Vincenzetti, V. and Martin, S. G. (2019). Sterol flow between the plasma membrane and the endosome is regulated by the LAM family protein Ltc1. *bioRxiv*, 720383. doi:10.1101/720383

Matsuyama, A., Shirai, A., Yashiroda, Y., Kamata, A., Horinouchi, S. and Yoshida, M. (2004). pDUAL, a multipurpose, multicopy vector capable of chromosomal integration in fission yeast. *Yeast* **21**, 1289-1305. doi:10.1002/yea.1181

Matsuyama, A., Shirai, A. and Yoshida, M. (2008). A series of promoters for constitutive expression of heterologous genes in fission yeast. *Yeast* **25**, 371-376. doi:10.1002/yea.1593

Maundrell, K. (1990). nmt1 of fission yeast. A highly transcribed gene completely repressed by thiamine. *J. Biol. Chem.* **265**, 10857-10864.

Maundrell, K. (1993). Thiamine-repressible expression vectors pREP and pRIP for fission yeast. *Gene* **123**, 127-130. doi:10.1016/0378-1119(93)90551-D

Meister, P., Taddei, A., Ponti, A., Baldacci, G. and Gasser, S. M. (2007). Replication foci dynamics: replication patterns are modulated by S-phase checkpoint kinases in fission yeast. *EMBO J.* **26**, 1315-1326. doi:10.1038/sj.emboj.7601538

Merlini, L., Khalili, B., Dudin, O., Michon, L., Vincenzetti, V. and Martin, S. G. (2018). Inhibition of Ras activity coordinates cell fusion with cell–cell contact during yeast mating. *J. Cell Biol.* **217**, 1467-1483. doi:10.1083/jcb.201708195

Moreno, M. B., Durán, A. and Ribas, J. C. (2000). A family of multifunctional thiamine-repressible expression vectors for fission yeast. *Yeast* **16**, 861-872. doi:10.1002/1097-0061(20000630)16:9<861::AID-YEA577>3.0.CO;2-9

Nguyen, A. N., Ikner, A. D., Shiozaki, M., Warren, S. M. and Shiozaki, K. (2002). Cytoplasmic localization of Wis1 MAPKK by nuclear export signal is important for nuclear targeting of Spc1/Sty1 MAPK in fission yeast. *Mol. Biol. Cell* **13**, 2651-2663. doi:10.1091/mbc.02-03-0043

Ohira, M. J., Hendrickson, D. G., Scott McIsaac, R. and Rhind, N. (2017). An estradiol-inducible promoter enables fast, graduated control of gene expression in fission yeast. *Yeast* **34**, 323-334. doi:10.1002/yea.3235

Onken, B., Wiener, H., Philips, M. R. and Chang, E. C. (2006). Compartmentalized signaling of Ras in fission yeast. *Proc. Natl. Acad. Sci. USA* **103**, 9045-9050. doi:10.1073/pnas.0603318103

Pédelacq, J.-D., Cabantous, S., Tran, T., Terwilliger, T. C. and Waldo, G. S. (2006). Engineering and characterization of a superfolder green fluorescent protein. *Nat. Biotechnol.* **24**, 79-88. doi:10.1038/nbt1172

Riedl, J., Crevenna, A. H., Kessenbrock, K., Yu, J. H., Neukirchen, D., Bista, M., Bradke, F., Jenne, D., Holak, T. A., Werb, Z. et al. (2008). Lifeact: a versatile marker to visualize F-actin. *Nat. Methods* **5**, 605-607. doi:10.1038/nmeth.1220

Sato, M., Dhut, S. and Toda, T. (2005). New drug-resistant cassettes for gene disruption and epitope tagging in Schizosaccharomyces pombe. *Yeast* **22**, 583-591. doi:10.1002/yea.1233

Siam, R., Dolan, W. P. and Forsburg, S. L. (2004). Choosing and using Schizosaccharomyces pombe plasmids. *Methods* **33**, 189-198. doi:10.1016/j.ymeth.2003.11.013

Siow, C. C., Nieduszynska, S. R., Müller, C. A. and Nieduszynski, C. A. (2012). OriDB, the DNA replication origin database updated and extended. *Nucleic Acids Res.* **40**, D682-D686. doi:10.1093/nar/gkr1091

Smith, G. (1976). Evolution of repeated DNA sequences by unequal crossover. *Science* **191**, 528-535. doi:10.1126/science.1251186

Snaith, H. A., Samejima, I. and Sawin, K. E. (2005). Multistep and multimode cortical anchoring of tea1p at cell tips in fission yeast. *EMBO J.* **24**, 3690-3699. doi:10.1038/sj.emboj.7600838

Strope, P. K., Kozmin, S. G., Skelly, D. A., Magwene, P. M., Dietrich, F. S. and McCusker, J. H. (2015). 2μ plasmid in Saccharomyces species and in Saccharomyces cerevisiae. *FEMS Yeast Res.* **15**, fov090. doi:10.1093/femsyr/fov090

Subach, O. M., Cranfill, P. J., Davidson, M. W. and Verkhusha, V. V. (2011). An enhanced monomeric blue fluorescent protein with the high chemical stability of the chromophore. *PLoS ONE* **6**, e28674. doi:10.1371/journal.pone.0028674

Tang, X., Huang, J., Padmanabhan, A., Bakka, K., Bao, Y., Tan, B. Y., Cande, W. Z. and Balasubramanian, M. K. (2011). Marker reconstitution mutagenesis: a simple and efficient reverse genetic approach. *Yeast* **28**, 205-212. doi:10.1002/yea.1831

Tatebe, H., Nakano, K., Maximo, R. and Shiozaki, K. (2008). Pom1 DYRK regulates localization of the Rga4 GAP to ensure bipolar activation of Cdc42 in fission yeast. *Curr. Biol.* **18**, 322-330. doi:10.1016/j.cub.2008.02.005

Van Driessche, B., Tafforeau, L., Hentges, P., Carr, A. M. and Vandenhaute, J. (2005). Additional vectors for PCR-based gene tagging in Saccharomyces cerevisiae and Schizosaccharomyces pombe using nourseothricin resistance. *Yeast* **22**, 1061-1068. doi:10.1002/yea.1293

Vjestica, A., Merlini, L., Dudin, O., Bendezu, F. O. and Martin, S. G. (2016). Microscopy of fission yeast sexual lifecycle. *J. Vis. Exp.* e53801. doi:10.3791/53801

Vještica, A., Merlini, L., Nkosi, P. J. and Martin, S. G. (2018). Gamete fusion triggers bipartite transcription factor assembly to block re-fertilization. *Nature* **560**, 397-400. doi:10.1038/s41586-018-0407-5

Wach, A., Brachat, A., Pöhlmann, R. and Philippsen, P. (1994). New heterologous modules for classical or PCR-based gene disruptions inSaccharomyces cerevisiae. *Yeast* **10**, 1793-1808. doi:10.1002/yea.320101310

Wang, C.-H., Balasubramanian, M. K. and Dokland, T. (2004). Structure, crystal packing and molecular dynamics of the calponin-homology domain of Schizosaccharomyces pombe Rng2. *Acta Crystallogr. D Biol. Crystallogr.* **60**, 1396-1403. doi:10.1107/S0907444904012983

Watson, A. T., Daigaku, Y., Mohebi, S., Etheridge, T. J., Chahwan, C., Murray, J. M. and Carr, A. M. (2013). Optimisation of the Schizosaccharomyces pombe urg1 expression system. *PLoS ONE* **8**, e83800. doi:10.1371/journal.pone.0083800

Watt, S., Mata, J., López-Maury, L., Marguerat, S., Burns, G. and Bähler, J. (2008). urg1: a uracil-regulatable promoter system for fission yeast with short induction and repression times. *PLoS ONE* **3**, e1428. doi:10.1371/journal.pone.0001428

Yamagishi, Y., Sakuno, T., Goto, Y. and Watanabe, Y. (2014). Kinetochore composition and its function: lessons from yeasts. *FEMS Microbiol. Rev.* **38**, 185-200. doi:10.1111/1574-6976.12049

Zhang, D., Vjestica, A. and Oliferenko, S. (2010). The cortical ER network limits the permissive zone for actomyosin ring assembly. *Curr. Biol.* **20**, 1029-1034. doi:10.1016/j.cub.2010.04.017

Zilio, N., Wehrkamp-Richter, S. and Boddy, M. N. (2012). A new versatile system for rapid control of gene expression in the fission yeast Schizosaccharomyces pombe. *Yeast* **29**, 425-434. doi:10.1002/yea.2920

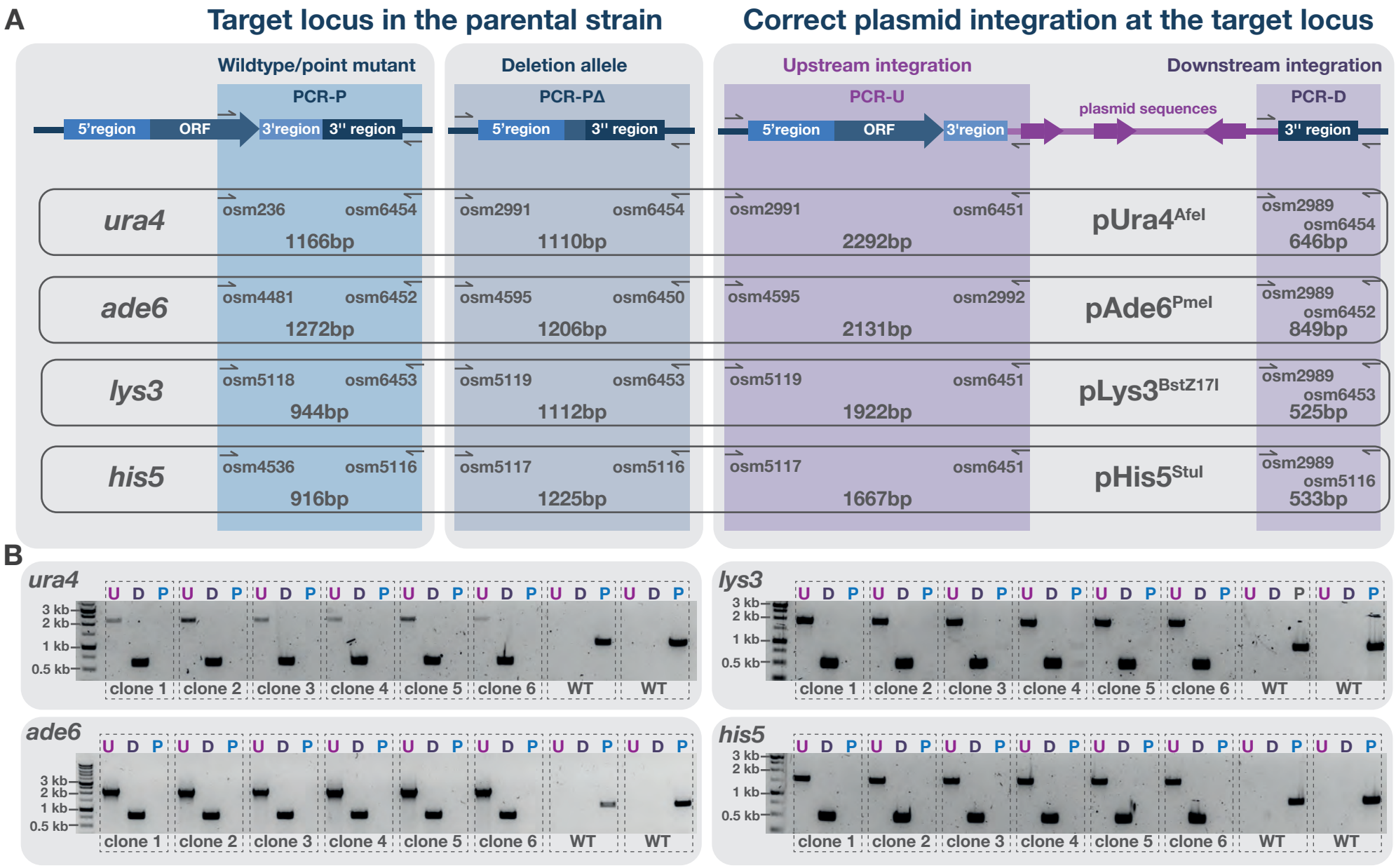

Figure S1. Diagnostic PCRs to test SIV genomic integration

(A) Overview of the genotyping strategy to test for correct integration of the plasmids targeting the indicated genomic loci. The top schematic shows parental and transformant loci where arrows denote the primers used for genotyping and colored areas the segment amplified by PCRs. The specific primers carrying the "osm" identifier, and the sizes of the PCR fragments they produce are denoted for each genomic locus. For primer sequences please see Supplemental Table S3. The left and middle panel show the diagnostic PCR for the presence of the parental locus. The PCR-P is used when transformants are obtained from wildtype and point-mutant target alleles, and PCR-PΔ when the parental strain is a deletion of the target locus (*ura4-D18*, *ade6-D19*, *lys3-D20*, *his5-D21*). The right panel shows the diagnostic PCRs to test for the correct upstream (PCR-U) and downstream (PCR-D) integration of the plasmids into target loci. **(B)** The PCR-U, PCR-D and PCR-P results performed on transformants at the indicated loci (clones 1-6) and the parental strain (WT) as detailed in (A).

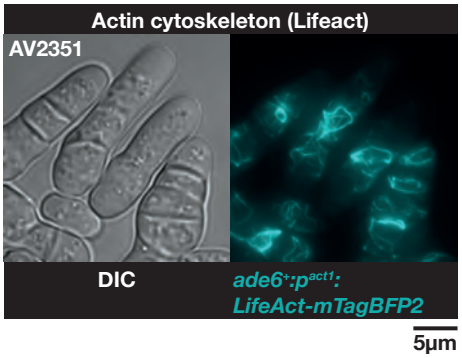

Figure S2. Aberrant F-actin upon expression of LifeAct-mTagBFP2

Micrographs of cells expressing LifeAct-mTagBFP2, showing aberrant actin cytoskeleton organization.

Table S1. List of plasmids used in the study. Please note embedded links to NBRP and Addgene repositories.

Addgene ID	NBRP ID	Plasmid ID	Plasmid name
133467	FYP4650	**pAV0133**	pUra4^{AfeI}
133468	FYP4651	**pAV0356**	pAde6^{PmeI}
133469	FYP4652	**pAV0357**	pLys3^{BstZ17I}
133470	FYP4653	**pAV0413**	pHis5^{StuI}
133471	FYP4654	**pAV0584**	pUra4^{AfeI}-natMX
133472	FYP4655	**pAV0585**	pAde6^{PmeI}-hphMX
133473	FYP4656	**pAV0586**	pLys3^{BstZ17I}-bsdMX
133474	FYP4657	**pAV0587**	pHis5^{StuI}-bleMX
133475	FYP4658	**pAV0784**	pHis5^{StuI}-bsdMX
133476	FYP4659	**pAV0661**	pAde6^{PmeI}-p^{act1}-sfGFP-terminator^{ScCYC1}
133477	FYP4660	**pAV0662**	pLys3^{BstZ17I}-p^{act1}-sfGFP-terminator^{ScCYC1}
133478	FYP4661	**pAV0663**	pHis5^{StuI}-p^{act1}-sfGFP-terminator^{ScCYC1}
133479	FYP4662	**pAV0714**	pUra4^{AfeI}-p^{act1}-sfGFP-terminator^{ScCYC1}
133480	FYP4663	**pAV0746**	pUra4^{AfeI}-p^{rga3}-sfGFP-terminator^{ScCYC1}
133481	FYP4664	**pAV0747**	pUra4^{AfeI}-p^{pom1}-sfGFP-terminator^{ScCYC1}
133482	FYP4665	**pAV0748**	pUra4^{AfeI}-p^{pak1}-sfGFP-terminator^{ScCYC1}
133483	FYP4666	**pAV0749**	pUra4^{AfeI}-p^{tdh1}-sfGFP-terminator^{ScCYC1}
133484	FYP4667	**pAV0750**	pUra4^{AfeI}-p^{urg1}-sfGFP-terminator^{ScCYC1}
133485	FYP4668	**pAV0751**	pUra4^{AfeI}-p^{nmt1}-sfGFP-terminator^{ScCYC1}
133486	FYP4669	**pAV0752**	pUra4^{AfeI}-p^{nmt41}-sfGFP-terminator^{ScCYC1}
133487	FYP4670	**pAV0753**	pUra4^{AfeI}-p^{nmt81}-sfGFP-terminator^{ScCYC1}
133488	FYP4671	**pAV0327**	pUra4^{AfeI}-p^{act1}-sfGFP-terminator^{tdh1}
133489	FYP4672	**pAV0328**	pUra4^{AfeI}-p^{act1}-mCherry-terminator^{tdh1}
133490	FYP4673	**pAV0471**	pUra4^{AfeI}-p^{tdh1*}-mTagBFP2-terminator^{tdh1}
133491	FYP4674	**pAV0624**	pUra4^{AfeI}-p^{tdh1}-3mTagBFP2-terminator^{tdh1}
133492	FYP4675	**pAV0517**	pHis5^{StuI}-p^{map3}-GFP-terminator^{nmt}
133493	FYP4676	**pAV0543**	pLys3^{BstZ17I}-p^{map3}-mCherry-terminator^{ScADH1}-natMX
133494	FYP4677	**pAV0761**	pLys3^{BstZ17I}-p^{map3}-mTagBFP2-terminator^{ScADH1}-bleMX
133495	FYP4678	**pAV0523**	pAde6^{PmeI}-p^{mam1*}-sfGFP-terminator^{ScADH1}-kanMX
133496	FYP4679	**pAV0762**	pAde6^{PmeI}-p^{mam1*}-mCherry-terminator^{ScADH1}-kanMX
133497	FYP4680	**pAV0763**	pAde6^{PmeI}-p^{mam1*}-mTagBFP2-terminator^{ScADH1}-kanMX
133498	FYP4681	**pAV0478**	pHis5^{StuI}-p^{tdh1}-NLS^{SV40}-sfGFP-NLS^{SV40}-natMX
133499	FYP4682	**pAV0479**	pHis5^{StuI}-p^{tdh1}-NES^{wis1}-sfGFP-NES^{mia1}-natMX
133500	FYP4683	**pAV0526**	pHis5^{StuI}-p^{tdh1}-sfGFP-NLS^{SV40}-natMX
133501	FYP4684	**pAV0765**	pLys3^{BstZ17I}-p^{tdh1}-NLS^{SV40}-mCherry-terminator^{ScADH1}-kanMX
133502	FYP4685	**pAV0532**	pLys3^{BstZ17I}-p^{tdh1}-NLS^{SV40}-mTagBFP2-terminator^{tdh1}-kanMX

Continued on the next page

Addgene ID	NBRP ID	Plasmid ID	Plasmid name
133503	FYP4686	**pAV0605**	pUra4^{AfeI}-p^{act1}-sfGFP-RitC-terminator^{tdh1}
133504	FYP4687	**pAV0607**	pAde6^{PmeI}-p^{act1}-mCherry-RitC-terminator^{ScADH1}
133505	FYP4688	**pAV0612**	pAde6^{PmeI}-p^{tdh1}-3mTagBFP2-RitC-terminator^{ScADH1}-bsdMX
133506	FYP4689	**pAV0620**	pUra4^{AfeI}-p^{pcn1}-eGFP-pcn1-terminator^{nmt1}-natMX
133507	FYP4690	**pAV0785**	pUra4^{AfeI}-p^{pcn1}-mCherry-pcn1-terminator^{nmt1}-natMX
133508	FYP4691	**pAV0756**	pHis5^{StuI}-p^{act1}-CRIB(gic2$^{aa2\text{-}181}$)-3mCherry-bsdMX
133509	FYP4692	**pAV0757**	pHis5^{StuI}-p^{pak1}-CRIB(gic2$^{aa2\text{-}181}$)-3GFP-terminator^{ScADH1}-kanMX
133510	FYP4693	**pAV0816**	pAde6^{PmeI}-p^{act1}-CRIB(gic2$^{aa2\text{-}181}$)-mTagBFP2-terminator^{ScADH1}-bsdMX
133511	FYP4694	**pAV0758**	pLys3^{BstZ17I}-p^{pak1}-RasAct(3xbyr2RBD)-3GFP-kanMX-terminator^{ScADH1}
133512	FYP4695	**pAV0835**	pUra4^{AfeI}-p^{act1}-mCherry-CHD^{Rng2}-terminator^{ScCYC1}
133513	FYP4696	**pAV0771**	pAde6^{PmeI}-p^{act1}-3mTagBFP2-CHD^{Rng2}-terminator^{ScCYC1}
133514	FYP4697	**pAV0782**	pAde6^{PmeI}-p^{act1}-LifeAct-sfGFP-terminator^{ScADH1}-bsdMX
133515	FYP4698	**pAV0783**	pAde6^{PmeI}-p^{act1}-LifeAct-mCherry-terminator^{ScADH1}-bsdMX
133516	FYP4699	**pAV0772**	pAde6^{PmeI}-p^{atb2}-sfGFP-atb2-terminator^{atb2}-hphMX
133517	FYP4700	**pAV0710**	pAde6^{PmeI}-p^{atb2}-mCherry-atb2-terminator^{atb2}-hphMX
133518	FYP4701	**pAV0770**	pAde6^{PmeI}-p^{atb2}-mTagBFP2-atb2-terminator^{atb2}-hphMX
133519	FYP4702	**pAV0773**	pLys3^{BstZ17I}-p^{BiP}-SignalSequence^{BiP}-sfGFP-AHDL-bsdMX
133520	FYP4703	**pAV0764**	pLys3^{BstZ17I}-p^{BiP}-SignalSequence^{BiP}-mCherry-AHDL-bsdMX
Not deposited	*Not deposited*	**pAV0569**	pUra4^{AfeI}-p^{tdh1*}-sfGFP-terminator^{tdh1}
Not deposited	*Not deposited*	**pAV0570**	pAde6^{PmeI}-p^{tdh1*}-sfGFP-terminator^{tdh1}
Not deposited	*Not deposited*	**pAV0571**	pLys3^{BstZ17I}-p^{tdh1*}-sfGFP-terminator^{tdh1}
Not deposited	*Not deposited*	**pAV0572**	pHis5^{StuI}-p^{tdh1*}-sfGFP-terminator^{tdh1}
Not deposited	*Not deposited*	**pAV0596**	pAde6^{PmeI}-ura4Casette
Not deposited	*Not deposited*	**pAV0597**	pLys3^{BstZ17I}-ura4Casette
Not deposited	*Not deposited*	**pAV0598**	pHis5^{StuI}-ura4Casette
Not deposited	*Not deposited*	**pAV0616**	pAde6^{PmeI}-ura4casette-hphMX
Not deposited	*Not deposited*	**pAV0617**	pLys3^{BstZ17I}-ura4casette-bsdMX
Not deposited	*Not deposited*	**pAV0618**	pHis5^{StuI}-ura4casette-bleMX
Not deposited	*Not deposited*	**pAV0623**	pJK210-natMX
Not deposited	*Not deposited*	**pAV0769**	pAde6^{PmeI}-p^{act1}-LifeAct-mTagBFP2-terminator^{ScADH1}-bsdMX

Table S2. List of fission yeast strains used in the study. Please note embedded links to NBRP repository.

NBRP ID	ID	Genotype	Description	Source
FY38487	**AV0890**	h⁻ ura4⁺:p^{act1}:sfGFP:terminator^{tdh1}	AV0880 was transformed with AfeI linearized pAV0327	This study
FY38488	**AV0891**	h⁻ ura4⁺:p^{act1}:mCherrry:terminator^{tdh1}	AV0880 was transformed with AfeI linearized pAV0328	This study
FY38489	**AV1196**	h⁺ ura4⁺:p^{tdh1*}:mTagBFP2:terminator^{tdh1}	AV0879 was transformed with AfeI linearized pAV0471	This study
FY38490	**AV1200**	h⁺ his5⁺:p^{tdh1}:NLS^{SV40}-sfGFP-NLS^{SV40}:natMX	ySM1371 was transformed with StuI linearized pAV0478	This study
FY38491	**AV1201**	h⁺ his5⁺:p^{tdh1}:NES^{wis1}-sfGFP-NES^{mia1}:natMX	ySM1371 was transformed with StuI linearized pAV0479	This study
FY38492	**AV1380**	h⁺ his5⁺:p^{tdh1}:sfGFP-NLS^{SV40}:natMX	AV1139 was transformed with StuI linearized pAV0526	This study
FY38493	**AV1382**	h⁺ his5⁺:p^{map3}:GFP:terminator^{nmt}	AV1139 was transformed with StuI linearized pAV0517	This study
FY38494	**AV1413**	h⁺ lys3⁺:p^{map3}:mCherry:natMX	ySM1371 was transformed with SpeI cut pAV0543	This study
FY38495	**AV1469**	h⁻ lys3⁺:p^{tdh1}:NLS-linker-mTagBFP2:terminator^{tdh1}:kanMX	ySM995 was transformed with SpeI linearizaed pAV0532	This study
FY38496	**AV1577**	h⁻ ura4⁺:p^{act1}:sfGFP-RitC:terminator^{tdh1} ade6-M210	AV0729 was transformed with AfeI linearized pAV0605	This study
FY38497	**AV1579**	h⁺ ade6⁺:p^{act1}:mCherry-RitC:terminator^{ScADH1} ura4-D18	AV1071 was transformed with PmeI linearized pAV0607	This study
FY38498	**AV1643**	h⁻ ade6⁺:p^{mam1*}:sfGFP:termintor^{ScADH1}:kanMX	ySM995 was transformed with RsrII/BamHI cut pAV0523	This study
FY38499	**AV1724**	h⁺ ade6⁺:p^{tdh1}:3mTagBFP2-RitC:terminator^{ScADH1}:bsdMX	ySM1371 was transformed with PmeI linearized pAV0612	This study
FY38500	**AV1725**	h^{90} ura4⁺:p^{pcn1}:eGFP-pcn1:3'UTR^{pcn1}:terminator^{nmt}:natMX	ySM1396 was transformed with AfeI linearized pAV0620	This study
FY38501	**AV1769**	h⁻ ura4⁺:p^{tdh1}:3mTagBFP2:terminator^{tdh1}	AV0153 was transformed with AfeI linearized pAV0624	This study
FY38502	**AV2295**	h⁻ ade6-D19	basic strain	This study
FY38503	**AV2296**	h⁺ ade6-D19	basic strain	This study
FY38504	**AV2297**	h⁻ ura4-D18	basic strain	This study
FY38505	**AV2298**	h⁺ ura4-D18	basic strain	This study
FY38506	**AV2300**	h⁻ lys3-D20	basic strain	This study
FY38507	**AV2301**	h⁺ lys3-D20	basic strain	This study
FY38508	**AV2302**	h⁻ his5-D21	basic strain	This study

NBRP ID	ID	Genotype	Description	Source
FY38509	**AV2303**	h^{+} his5-D21	basic strain	This study
FY38510	**AV2319**	h^{-} his5^{+}:p^{pak1}:CRIB$^{[gic2aa1-181]}$-3GFP-terminator^{ScADH1}:kanMX	AV2302 was transformed with StuI linearized pAV0757	This study
FY38511	**AV2320**	h^{+} lys3^{+}:p^{pak1}:RasAct-3GFP-terminator^{ScADH1}:kanMX	AV2301 was transformed with StuI linearized pAV0758	This study
FY38512	**AV2321**	h^{+} lys3^{+}:p^{BiP}:SignalSequence^{BiP}-sfGFP-AHDL:bsdMX	AV2301 was transformed with StuI linearized pAV0773	This study
FY38513	**AV2322**	h^{+} lys3^{+}:p^{tdh1}:NLS-linker-mCherry:terminator^{ScADH1}:kanMX	AV2301 was transformed with StuI linearized pAV0765	This study
FY38514	**AV2323**	h^{+} lys3^{+}:p^{BiP}:SignalSequence^{BiP}-mCherry-AHDL:bsdMX	AV2301 was transformed with StuI linearized pAV0764	This study
FY38515	**AV2324**	h^{-} his5^{+}:p^{act1}:CRIB$^{[gic2aa1-181]}$-3mCherry:bsdMX	AV2302 was transformed with StuI linearized pAV0756	This study
FY38516	**AV2327**	h^{+} lys3^{+}:p^{map3}:mTagBFP2:terminator^{ScAdh1}:bleMX	AV2301 was transformed with SpeI linearized pAV0761	This study
FY38517	**AV2349**	h^{-} ade6^{+}:p^{act1}:LifeAct-mCherry:terminator^{ScADH1}:bsdMX	AV2295 was transformed with RsrII/BlpI fragment of pAV0783	This study
FY38518	**AV2350**	h^{-} ade6^{+}:p^{act1}:LifeAct-sfGFP:terminator^{ScADH1}:bsdMX	AV2295 was transformed with RsrII/BlpI fragment of pAV0782	This study
FY38519	**AV2353**	h^{-} ade6^{+}:p^{act1}:3mTagBFP2-CHDRng2-terminator^{ScCYC1}	AV2295 was transformed with PmeI linearized pAV0771	This study
FY38520	**AV2356**	h^{-} ade6^{+}:p^{mam1*}:mCherry:terminator^{ScADH1}:kanMX	AV2295 was transformed with RsrII/BlpI fragment of pAV0762	This study
FY38521	**AV2357**	h- ade6^{+}:p^{mam1*}:mTagBFP2:terminator^{ScADH1}:kanMX	AV2295 was transformed with RsrII/BlpI fragment of pAV0763	This study
FY38522	**AV2362**	h^{90} ura4-D18	basic strain	This study
FY38523	**AV2387**	h^{-} ade6^{+}:p^{act1}:CRIB$^{[gic2aa1-181]}$-mTagBFP2:terminator^{ScADH1}:bsdMX	AV2343 was transformed with RsrII/BlpI fragment of pAV0816	This study
FY38524	**AV2388**	h^{-} ura4^{+}:p^{pcn1}:mCherry-pcn1:3'UTR^{pcn1}:terminator^{nmt}:natMX	AV2343 was transformed with AfeI linearized pAV0785	This study
FY38525	**AV2392**	h^{-} ade6^{+}:p^{atb2}:mCherry-atb2:terminator^{atb2}:hphMX	AV2343 was transformed witth PmeI linearized pAV0710	This study
FY38526	**AV2433**	h^{-} ade6^{+}:p^{atb2}:mTagBFP2-atb2:terminator^{atb2}:hphMX	AV2343 was transformed witth PmeI linearized pAV0770	This study
FY38527	**AV2434**	h^{-} ade6^{+}:p^{atb2}:sfGFP-atb2:terminator^{atb2}:hphMX	AV2343 was transformed witth PmeI linearized pAV0772	This study
FY38528	**AV2453**	h^{-} ura4^{+}:p^{act1}:mCherry-CHDRng2:terminator^{ScCYC1}	AV0153 was transformed with AfeI linearized pSM2436	This study

NBRP ID	ID	Genotype	Description	Source
Not deposited	**ySM995**	h^- wildtype	Fission yeast strain 972	Lab stock
Not deposited	**ySM1371**	h^+ wildtype	Fission yeast strain 975	Lab stock
Not deposited	**ySM1396**	h^{90} wildtype	Fission yeast strain 968	Lab stock
Not deposited	**ySM1131**	h^- pak2Δ:ura4+ leu1-32 ura4-D18		Lab stock
Not deposited	**AV0138**	h^{90} pak2Δ:ura4+ ura4+		Lab stock
Not deposited	**AV0226**	h^+ myo52Δ:ura4+ pak2Δ:ura4+ ura4+		Lab stock
Not deposited	**yMM625**	h^+ ltc1-sfGFP:kanMX ura4$^+$:p^{act1}:D4H-mCherry		Lab stock
Not deposited	**yMM1032**	h^+ ltc1Δ:hphMX ura4$^+$:p^{rga3}:ltc1-sfGFP ade6$^+$:p^{act1}:mCherry-D4H		Lab stock
Not deposited	**yMM1036**	h^+ ltc1Δ:hphMX ura4$^+$:p^{pak1}:ltc1-sfGFP ade6$^+$:p^{act1}:mCherry-D4H		Lab stock
Not deposited	**yMM1034**	h^+ ltc1Δ:hphMX ura4$^+$:p^{pom1}:ltc1-sfGFP ade6$^+$:p^{act1}:mCherry-D4H		Lab stock
Not deposited	**yMM1015**	h^+ ltc1Δ:hphMX ura4$^+$:p^{act1}:ltc1-sfGFP ade6$^+$:p^{act1}:mCherry-D4H		Lab stock
Not deposited	**AV2351**	h^- ade6$^+$:p^{act1}:LifeAct-mTagBFP2:terminator^{ScADH1}:bsdMX	AV2295 was transformed with RsrII/BlpI fragment of pAV0782	Lab stock

Table S3. List of primers used for genotyping. See Figure S1 for usage.

Serial ID	Sequence	Tm (°C)	Length (bp)	GC %	GC Clamp	Secondary Structure	Primer Dimer	Extinction Coefficient
osm236	TCATCATTGTTGGTCGTGGAGTC	68.2	23	47.8	1	None	No	216.3
osm2989	GATTGTACTGAGAGTGCACCAT	60.7	22	45.5	2	Very Weak	No	217.6
osm2991	GTTGATGCCAGACCGTAATGAC	65.4	22	50	1	None	No	216.2
osm2992	CTGTGCGGTATTTCACACCGC	69.6	21	57.1	4	Very Strong	No	188.5
osm4481	GTATGGTTGCTGCAATGAC	59.1	19	47.4	1	Very Weak	No	182.7
osm4536	TTCTGAAGTCCCAAGCACG	64.1	19	52.6	2	None	No	179.8
osm4595	GCCTGGTGCAGTATAAGGTA	59.2	20	50	2	Weak	No	201.5
osm5116	GATAGTACAATTACGCATTCTG	55.6	22	36.4	1	Very Weak	No	219.3
osm5117	CATTTGGTAACCCGCAGTTGG	68.1	21	52.4	2	Very Weak	No	197.7
osm5118	TTGGCTTTGAAGGACGTCGAC	68.5	21	52.4	2	None	No	199.2
osm5119	CCGCATACTGACCAAAAGTGC	66.5	21	52.4	2	Weak	No	202.1
osm6450	CCTGAATAATGTGCTGTGAAGC	63.4	22	45.5	2	Weak	No	213.4
osm6451	TTCTCCTTACGCATCTGTGC	63	20	50	2	Weak	No	171.6
osm6452	TACCTTCCAAACATCGGACAG	63.8	21	47.6	1	Weak	No	202.9
osm6453	TTTCTTGAACATCTTGCTCGTG	64.1	22	40.9	2	None	No	195.8
osm6454	ACATTGGTAAACACTGTAAGTTCG	60.8	24	37.5	2	Very Weak	No	241.1

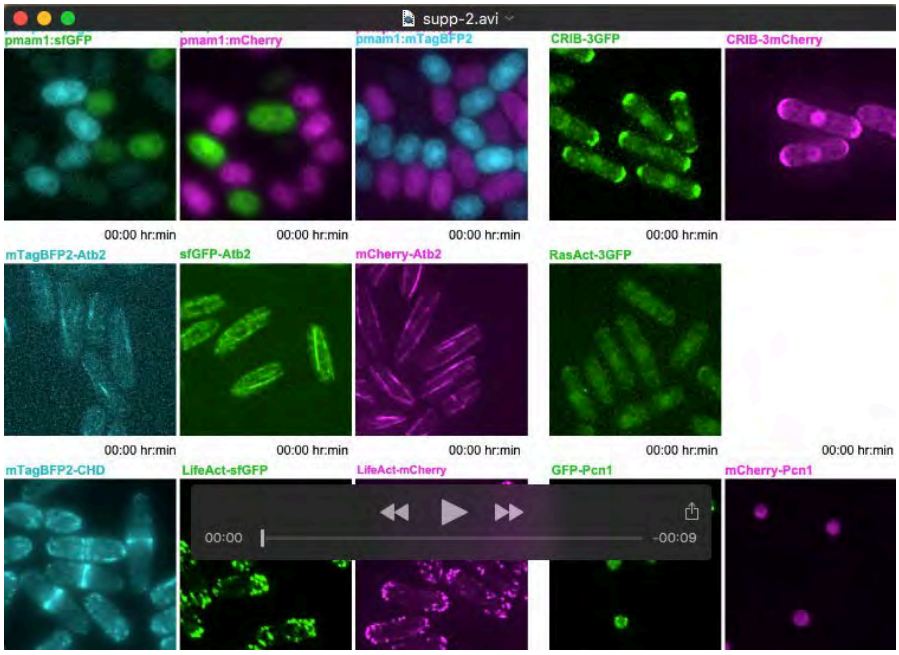

Movie 1. Timelapse images of cells expressing indicated fluorophores. Time in hour:min format is indicated at the top of each strain.